

1 Development of a Forced Advection Sampling Technique (FAST) for 2 Quantification of Methane Emissions from Orphaned Wells

3 Mohit L. Dubey¹, Andre Santos², Andrew B. Moyes², Ken Reichl², James E. Lee³, Manvendra K.
4 Dubey³, Corentin LeYhuelic⁴, Evan Variano¹, Emily Follansbee³, Fotini K. Chow¹, Sébastien C. Biraud²

5
6 ¹ Department of Environmental Engineering, University of California, Berkeley, CA, 94720, USA

7 ² Lawrence Berkeley National Laboratory, Berkeley, CA, 94720, USA

8 ³ Los Alamos National Laboratory, Los Alamos, NM, 87545, USA

9 ⁴ Ecole Normale Supérieure Paris Saclay, Paris, France

10 *Correspondence to:* Mohit L. Dubey (mldubey96@berkeley.edu)

11 Abstract.

12 Orphaned wells, meaning unplugged and non-producing wells lacking responsible owners, pose a significant and
13 undersampled environmental challenge due to their vast number and unknown associated emissions. We propose, develop,
14 and test an alternative method for estimating emissions from orphaned wells using a Forced Advection Sampling Technique
15 (FAST) that can overcome many of the limitations in current methods (cost, accuracy, safety). In contrast to existing ambient
16 Gaussian plume methods, our approach uses a fan-generated flow to force advection between the emission source and a point
17 methane (CH₄) sensor. The fan flow field is characterized using a colocated sonic anemometer to measure the 3D wind
18 profile generated by the fan. Using time-series measurements of CH₄ concentration and wind, a simple estimate of the CH₄
19 emission rate of the source can be inferred. The method was calibrated using outdoor controlled release experiments and then
20 tested on four orphaned wells in Lufkin, TX, and Osage County, OK. Our results suggest that the FAST method can provide
21 a low-cost, portable, fast and safe alternative to existing methods with reasonable estimates of orphaned well emissions over
22 a range of leak rates below 40 g/h and within certain geometric and atmospheric constraints.

23 1 Introduction

24 1.1 Motivation

25 Orphaned oil and gas wells, meaning unplugged and non-producing wells lacking responsible owners, pose a
26 significant and undersampled environmental challenge. In the United States (U.S.) alone, there are approximately 120,000
27 documented orphaned wells [Merrill et al., 2023], with an estimated 310,000 to 800,000 more undocumented wells [IOGCC,
28 2021]. For much of the 20th century, orphaned wells were considered a non-issue compared to active wells, as they were
29 thought to have low emission rates, particularly when they were reported as “plugged”. However, existing estimates of total
30 orphaned well emissions are based only on direct measurements of <0.03% of known wells [Kang et al., 2023], making them
31 a highly undersampled and uncertain source of anthropogenic methane (CH₄). CH₄ is a potent greenhouse gas with a global
32 warming potential (GWP) 84 times higher than carbon dioxide (CO₂) taken over 20 years [IEA] and a relatively short

lifetime (8-11 yrs) making it a high priority in combating near-term global warming. Based on a database of leak measurements at 598 wells across the U.S. and Canada, it was found that “annual methane emissions from abandoned wells are underestimated by 150% in Canada and by 20% in the U.S.” [Williams et al., 2021]. This lack of reliable emission data has resulted in increased interest in measuring and plugging orphaned wells as an important area of research for methane emissions reduction and near term climate change mitigation [O’Malley, 2024].

Alongside academia, the political sphere has shown increased interest in measuring and plugging orphaned wells. The Global Methane Pledge was signed at COP26 in 2021 by 155 countries representing over 50% of global CH₄ emissions who committed to 30% reductions of emissions from 2020 levels by 2030 [UNFCCC Secretariat, 2022]. The U.S. has since begun to investigate plugging orphaned wells, with an investment of \$660 million in 2023 through the Department of Interior [DOI, 2023]. From 2018-2020, the average cost of plugging a single well in the U.S. ranged from \$2,400 to \$227,000, with an overall three-year average of \$25,634 [IOGCC, 2021]. Using these numbers directly, without adjusting for inflation or overhead costs, this funding would be sufficient for plugging around 25,000 wells, or only 20% of the documented orphaned wells and a mere 3% of the upper bound of total orphaned wells. Given the high-cost of surveying and plugging, it will be critical to prioritize wells with larger emissions to reduce the economic burden of plugging orphaned wells.

Estimating emissions from orphaned wells is challenging due to their remote locations and typically low emission rates. Based on the aforementioned database of 598 wells across the U.S. and Canada, it has been estimated that orphaned well emission rates range from less than 1 to 48 g/h per well, with an average of around 6 g/h [Williams et al., 2021]. However, recent measurements in the US have also shown abandoned orphaned well emissions exceeding 1 kg/h with a mean value of 138 g/h [Follansbee et al., 2024, Riddick et al., 2024]. Still, extremely high-emitting orphaned wells are very rare and the vast majority of wells emit below the thresholds needed to observe them using current remote sensing platforms [Sherwin et al., 2024].

There are a variety of ground-based measurement approaches that can be applied to measure emissions from orphaned wells (Table 1). These range from expensive hand-held forward looking infrared cameras (FLIR) to more time-intensive mobile (OTM-33a) [U.S. EPA, 2014] and stationary systems (SEMTECH Hi-Flow 2 [SEMTECH], Chamber [Williams et al. 2023], Gaussian Plume Modeling (GPM) [Lushi and Stockie, 2010], Vent [Ventbusters, 2023]). Unmanned aerial vehicles (UAV, also known as “drones”) have also recently been proposed as a means of measuring wells, and preliminary results look promising [Dooley et al., 2024]. However, due to the expensive or complex nature of most of these methods only <0.03% of orphaned wells have been sampled. To overcome this data gap, new robust and fast techniques for estimating emission rates on the order of 1-10s g/h are needed (i.e. FAST).

Previous studies have investigated existing methods for quantifying methane emissions on the order of those relevant for studying orphaned wells [Dubey et al., 2023, Riddick et al., 2023, 2022]. Table 1 shows a list of the existing technologies that can measure methane emissions in this regime and their relative costs and sensitivities. The existing methods that are accurate and portable enough for measuring orphaned wells have other limitations, including insensitivity (FLIR), high-cost (SEMTECH), complexity and safety (Chamber [Riddick et al., 2023], Vent [Ventbusters, 2023], UAV [Dooley et al., 2024], OTM-33a [Edie et al., 2020]), accuracy, hardware and labor costs that are summarized in Table 1. Therefore, there is a pressing need for a cost-effective, efficient, safe and accurate method using existing sensors to estimate methane emissions for prioritizing orphaned well plugging. Although the FAST method is currently relatively expensive and difficult to set up/transport, it could be considered safer than many approaches, will work in complex aerodynamic environments, and could be used to quantify emissions from larger pieces of infrastructure such as abandoned pump jack wells that won't fit in a chamber or are surrounded by trees.

Method	FLIR Camera	SEMTECH HI-Flow 2	Static Chamber	Dynamic Chamber	GPM	Vent	UAV	OTM-33a	FAST
Hardware Cost	>\$50K	~\$40K	>\$400	>\$400	>\$5K	~\$50K	>\$50K	>\$10K	\$50K*
Range (g/h)	N/A	<1-30,000	>0.1	>0.1	>100	>100	>50	>50	>1
Uncertainty	N/A	±10%	-50%, +100%	±15%	±40%	N/A	N/A	±70%	±50%
Size (L)	~0.3	~15	~20	~20	~50	N/A	~40	>1,000	~50
Measuring Time (min.)	~2	~3	>30	>30	>10	>30	>30	>10	~3
Setup Time (min.)	~5	~5	>10	>10	>10	>10	>30	>30	~30

Table 1: Comparative assessment of commercial (FLIR, SEMTECH Hi-Flow 2, Vent) and research (Chamber, GPM, UAV, OTM-33a) methods used to monitor fugitive methane leaks from orphaned wells. Hardware costs, detection range, accuracy, size, labor and safety are compared for each technology. *The FAST method in this study is currently limited by the high cost of laser trace gas sensors (Picarro, Aeris, etc.) that can be reduced significantly by using cheaper non-laser sensors (i.e. Gas Rover) used in chambers.

84

85 In this paper, we propose, develop, and test a novel method for estimating CH₄ emissions from orphaned wells
86 using a Forced Advection Sampling Technique (FAST) that can overcome many of the limitations of other methods, as
87 outlined in Table 1. In contrast to existing ambient Gaussian plume methods (GPM), our approach uses a fan-generated flow
88 to force advection between the emission source and a point sensor. This eliminates the need for an estimate of atmospheric
89 stability, which is required to use the GPM. Using a colocated anemometer to measure the 3D wind profile generated by the
90 fan, a simple estimate of the CH₄ emission rate of the source can be obtained. The method is calibrated using an outdoor
91 controlled release experiment and blindly tested on four wells in Lufkin, TX, and Osage County, OK. We report results that
92 suggest that the FAST method can potentially provide a low-cost, portable, fast and safe alternative to existing methods to
93 provide reasonable estimates of orphaned well emissions under reasonable meteorological conditions.

94

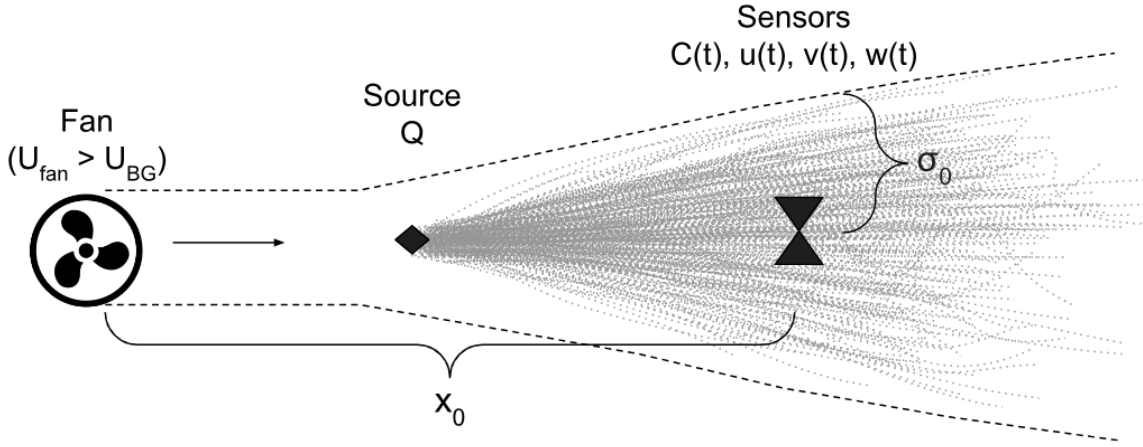
95 1.2 Mathematical Model

96 The physics underlying the FAST approach is based on a steady-state solution to the advection-diffusion equation.
97 This solution, known as the Gaussian plume equation [Veigle and Head, 1978] has been widely used in the literature to
98 perform emission inversions. However, previous studies using the Gaussian plume equation consider larger emission sources
99 and length scales (> 2 meters) than those of interest in this study [Snoun et al., 2023] [Perry et al., 2005]. As a result,
100 traditional GPM studies are typically dependent on parametrizations (i.e. Pasquill stability class), which are too coarse for
101 the length and time scales used when studying orphaned wells at smaller (on the order of a meter) length scales.
102 Furthermore, most previous studies using the GPM approach use ambient winds as opposed to a fan-generated plume within
103 an ambient background. In one exception to this, an approach to localize emissions using a fan-generated flow was devised
104 by [Sanchez-Sosa et al., 2018]. However this approach was only tested indoors and did not estimate emissions for their
105 source of interest (ethanol).

106

107 Here we outline the underlying physics of scalar transport within a jet of fan-generated turbulent flow and derive a
108 linear equation that can be used to estimate the emission rate of a source from time-averaged centerline measurements of
109 concentration and wind velocity within that flow.

110



111

112 **Figure 1:** Schematic of the FAST method where an upwind fan (with mean downwind speed U_{fan} larger than the background
 113 U_{BG}) generates a turbulent jet to advect a non-reactive gas (CH_4) leaking at volumetric flow rate (Q) from a source to
 114 downwind sensors (anemometer measuring $u(t), v(t), w(t)$ and CH_4 analyzer measuring $C(t)$).

115

116 The method assumes a constant emission source with emission rate Q (g/s) positioned downstream from a fan
 117 aligned with the mean background wind direction, where the velocity of the fan flow (U_{fan}) is larger than that of the
 118 background wind (U_{BG}). Adding this fan creates an environment which is assumed to have homogeneous turbulence between
 119 the source and the sensors. The sensors are positioned downstream along the centerline from the fan by a distance (x_0) and
 120 measure time series of concentration (C) and velocity (u, v, w).

121

122 The estimated emission rate (\hat{Q}) is calculated by integrating the scalar flux ($C \cdot u$) over a circular cross-section (dA)
 123 at some downstream location.

124

$$Q = \oint C u dA \approx \underline{C_{CL}} \underline{u_{CL}} \pi \sigma_0^2$$

125

$$\hat{Q} = \underline{C_{CL}} \underline{u_{CL}} \pi \sigma_0^2 \quad (1)$$

126

127 where spatial averages of concentration and velocity are approximated with time averages (underline) of centerline
 128 measurements (subscript "CL"). This gives a radial distance (σ_0) which is approximately the effective width of the plume at
 129 the downwind distance x_0 . This radial distance σ_0 is estimated based on a previous study of fan-generated flows [Halloran et.
 130 al, 2014] as a form of turbulent transport [Taylor, 1922]. Halloran et al. showed that the expansion of a fan-generated plume
 131 close to the source is proportional to the square root of the downwind distance and dependent on the turbulence intensity
 132 (i_{fan}) and characteristic length scale (l_{fan}) of the fan:

133

134

$$\sigma \sim (i_{fan} l_{fan} x)^{\frac{1}{2}}$$

135

$$\sigma_0 = (\beta i_{fan} l_{fan} x_0)^{\frac{1}{2}} \quad (2)$$

136

137 Evaluating Equation 2 at location x_0 and combining with Equation 1, \hat{Q} can be rewritten as a linear function of time-averaged
138 centerline concentration and velocity measurements:

139

140

$$\hat{Q} = \pi \beta i_{fan} l_{fan} x_0 \underline{C_{CL}} \underline{u_{CL}} = K_{FAST} \underline{C_{CL}} \underline{u_{CL}} \quad (3)$$

141

142 where the proportionality constant (K_{FAST}) is only dependent on constants related to the fan and the geometry of the system β
143 (which is treated in more detail in Appendix A):

144

145

$$K_{FAST} = \pi \sigma_0^2 = \pi \beta i_{fan} l_{fan} x_0 \quad (4)$$

146

147 2 Methods

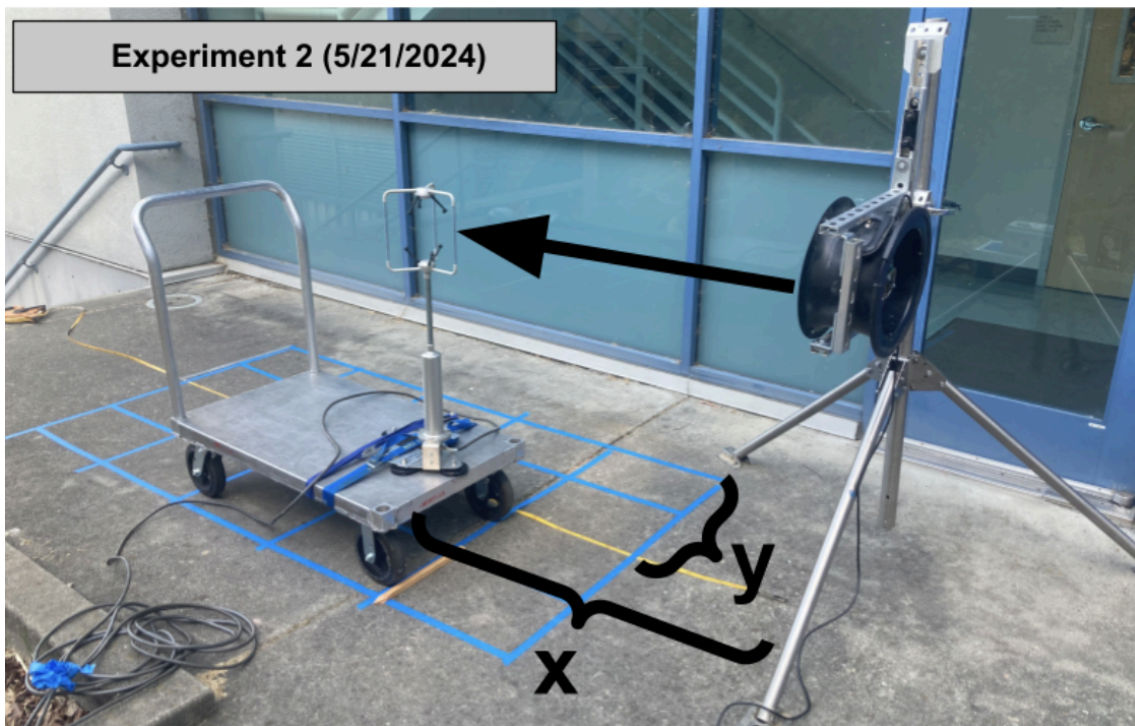
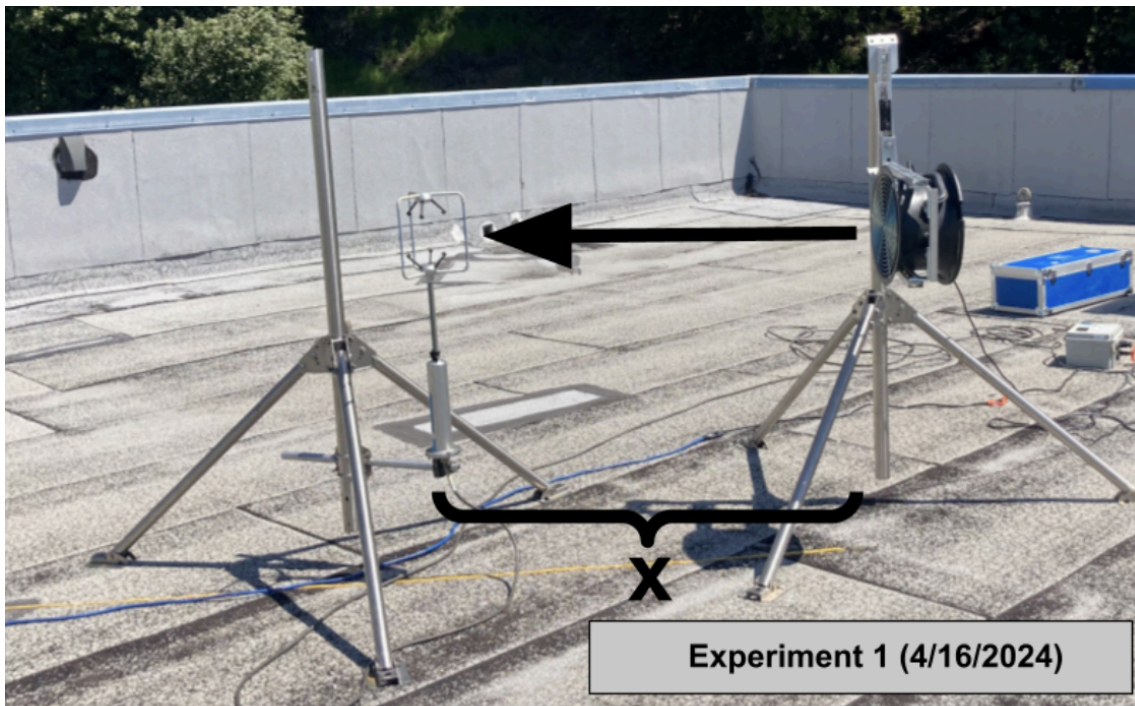
148 2.1 Fan Characterization Experiments

149 To characterize the effectiveness of using a fan to generate a turbulent jet for the FAST method, experiments were conducted
150 at Lawrence Berkeley National Lab (LBNL) on the afternoon of 4/16/2024 and in the morning of 5/21/2024 (Figure 2). For
151 both experiments, a Gill Windmaster (United Kingdom) 3-D sonic anemometer was used to collect 3-D wind speed
152 measurements at 10 Hz downwind of a Minneapolis Duct Blaster (MDB) fan with no attachments. This fan was chosen as it
153 is similar to those used in Halloran et al. and can be easily operated in the field at multiple fan speeds controlled by a dial.
154 Both the fan and the anemometer were mounted on tripods at a height of 1 meter. For these experiments, u is aligned to be in
155 the x direction (upwind/downwind), v in the y direction (crosswind) and w in the z direction (vertical).

156

157 A key assumption of this study is that the effective plume width (σ_0) derived in Halloran et al. (2014) for smoking oil
158 plumes is applicable to methane dispersion from orphaned wells. While the MDB fan generates turbulent transport similar to
159 Halloran et al., differences in the physical properties of smoking oil and methane—such as buoyancy, diffusion rates, and
160 emission dynamics—could lead to deviations in plume behavior. These potential differences underscore the need for

161 additional experiments designed specifically for methane to validate the use of (σ_0) under these conditions and further refine
162 the FAST method's applicability.
163
164 During the first experiment, measurements were taken for nine-minute intervals at downwind distances of 0.5 - 5 meters for
165 two different fan speed settings, referred to as “Low” (~ 3 m/s on average at a distance of 1 m) and “High” (~ 5 m/s on
166 average at a distance of 1 m). The system was set up to be aligned to the background wind of ~ 3 m/s from West-NorthWest.
167 Despite attempts to align the fan with the dominant background wind direction, there were still persistent crosswind gusts on
168 the order of ~ 1 m/s which varied as the experiment progressed. Moreover, the vertical velocity (w) was higher than expected
169 for two main reasons: the anemometer is mounted at a height of 1 meter and the experiment was conducted on a rooftop.
170 While w should be ~ 0 m/s at ground level, we measured w on the order of ~ 1 m/s due to these factors.
171



172
 173 **Figure 2:** Experimental setup for fan characterization experiments, using an anemometer placed at a downwind distance x
 174 and crosswind distance y (second experiment)

175

176 2.2 Controlled Release Experiment

177

178 To verify and estimate the relevant parameters used in the FAST method, a controlled release experiment was conducted
179 using a range of constant methane leak rates. The SEMTECH HI-FLOW backpack system was used for verification as it has
180 already been validated as a commercial product for estimating leak rates (see Appendix B for more details).

181

182 2.2.1 Experimental Setup

183

184 The fan position, source position, and sampling position were all 1 meter above ground level, and 1 meter separated
185 from each other along an axis parallel to the ground, with the source placed in between the fan and the sample point (Figure
186 3). A methane source was prepared by mixing 75 psi of high purity CH₄ with 1425 psi ultra-high purity N₂ in a 30 L
187 aluminum cylinder, to obtain a blend of $5.0 \pm 0.17\%$. The source was released from the cylinder at controlled rates using a
188 regulator plumbed through a mass flow controller (Brooks Instrument GF40) programmed with set points corresponding to
189 planned CH₄ emission rates of 1, 2, 5, 10, 20, and 40 g/hr. The sampling for the FAST method was conducted using a Picarro
190 G4302 analyzer [GasScouter™ G4302 Mobile Gas Concentration Analyzer] for measuring the CH₄ concentration and a
191 Gill Windmaster 3-D sonic anemometer placed as physically close together as possible at the sample position (inlet tube
192 mounted within 1 cm of center of anemometer, see Figure 3). The forced advection was done using an MDB fan with no
193 attachments. The fan, anemometer, and data collection systems were powered using a 300 Amp-hour 12V DC battery and
194 inverter, while the Picarro analyzer ran on its internal battery.

195

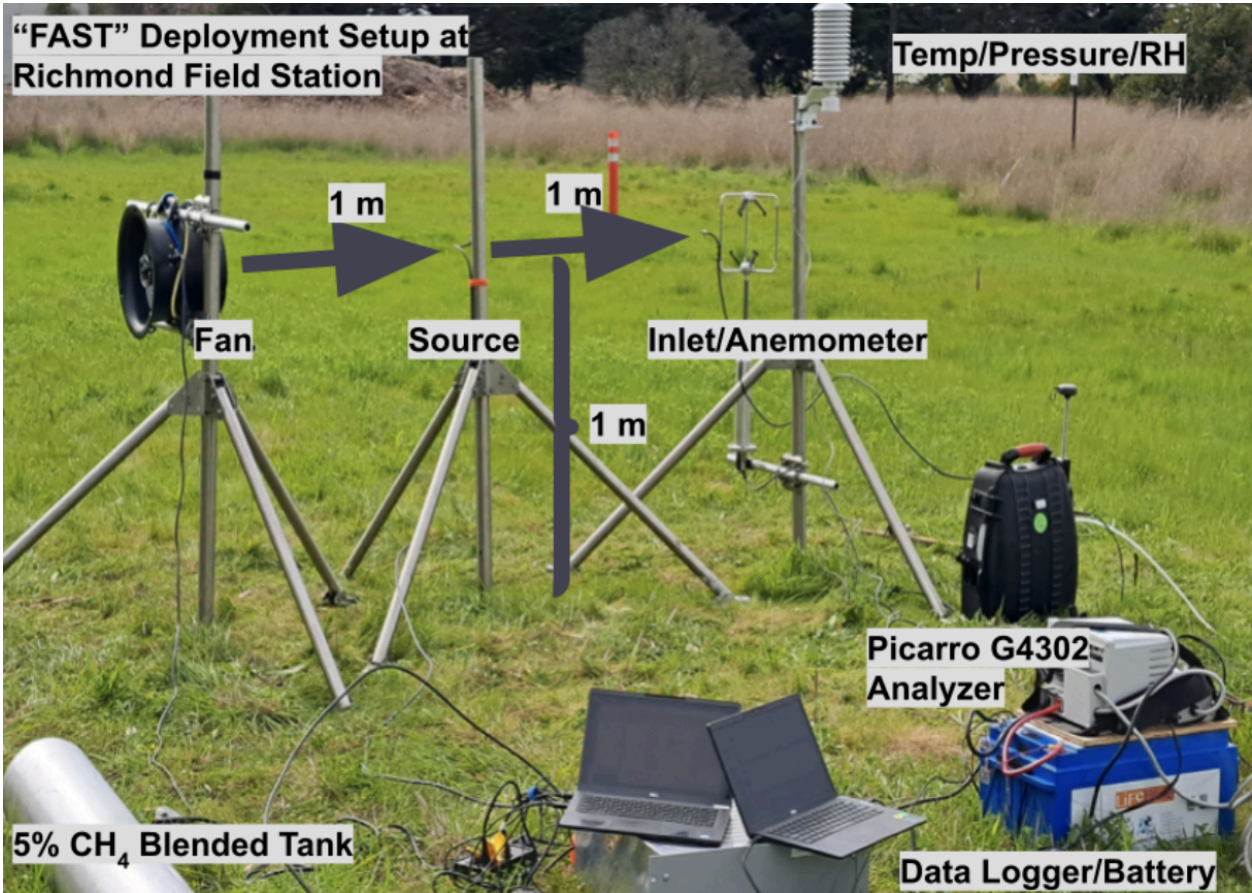
196 Sensor signals from wind, ambient air temperature, pressure, and source output flow were collected using data
197 loggers, with all data collection system clocks synchronized to within one second of UTC. The experiment began at 18:30
198 UTC with setup and preparation. At 20:19, the initial experiment for background (1.99 ± 0.36 ppm) measurements started
199 with no source emission. The experiment involved different flow rates with corresponding durations. For each flow rate
200 interval, the SEMTECH measurements were conducted in 2 minutes with no fan, followed by the FAST data collection with
201 10 minutes without the fan, 10 minutes with the fan at low intensity, and 5 minutes of the fan at high intensity, with 5 to 10
202 minutes of adjustment between flow rate steps to avoid transient periods. The experiment concluded at 00:21 UTC (the
203 following day).

204

Measured Quantity	Sensor	Measurement Frequency	Data Collection System	Associated System
CH ₄ (ppb)	Picarro G4302	2 Hz	Integrated computer	

			running Windows 7	FAST
u, v, w (m/s)	Gill Windmaster 1210-PK-085	10 Hz	Campbell Datalogger CR1000X	
Air Temperature (°C)	RM Young 41382VC	1 Hz		
Air Pressure (kPa)	Setra 278	1 Hz		
Source Flow (L/min.)	Brooks Instrument GF40	1 Hz	Campbell Datalogger CR6	Controlled Release

205 **Table 2:** Equipment used during the controlled release experiment at Richmond Field Station
 206



207
 208 **Figure 3:** Experimental setup for the controlled release experiment at Richmond Field Station in Richmond, CA. The MDB
 209 fan, the inlet for the Picarro G4302 analyzer and the Gill Windmaster 3-D sonic anemometer were mounted at 1 m height at
 210 a distance of 2 m from one another (upper limit for the FAST method). A source of 5% methane blended with pure nitrogen

was also mounted on a second tripod at a downwind distance of 1 m from the fan and outfitted with a piece of foam to ensure diffuse emissions.

213

214 2.2.2 Stoichiometry

215

The methane source leak rates in g/hr are calculated using measured quantities of source flow, ambient air temperature, pressure, and assumed constant source concentration. The measured quantities reported for each step were averaged over each measurement. The source leak rate Q is described in terms of measured quantities and known constants.

$$219 \quad Q = C \rho \kappa \quad (5)$$

220 where, C is the CH_4 concentration from the source tank at 0.05 ± 0.0017 [mol CH_4 / mol air], ρ is the CH_4 mass density [g/L] at measured ambient temperature and pressure, and

222 κ is the corrected output mass flow of the source gas.

223

224 The CH_4 mass density is calculated in terms of measured qualities of ambient air pressure P and temperature T as

$$225 \quad \rho = (M_{\text{CH}_4}/R)(P/T)$$

226 where, M_{CH_4} is molar mass 0.01604 [Kg / mol] of CH_4 , and R is the universal gas constant 8.31446 [(L · kPa)/(K · mol)].

227 The corrected output mass flow κ is calculated from the measured flow rate κ_{std} reported at standard temperature T_{std} of 293 Kelvin and measured ambient temperature T as

$$229 \quad \kappa = \kappa_{\text{std}}(T/T_{\text{std}})$$

230

231 Rewriting Q in terms of measured quantities we find:

$$232 \quad Q = \alpha C P \kappa_{\text{std}} \quad (6)$$

233 where,

$$234 \quad \alpha = [M_{\text{CH}_4}/(RT_{\text{std}})]$$

235

236 The source leak rate uncertainty σ_Q (shown as error bars on Q estimates) is estimated from uncertainties in source concentration C , measured quantities of ambient air pressure P and output flow κ_{std}

$$238 \quad \sigma_Q = \alpha \sqrt{(P \kappa_{\text{std}} \sigma_C)^2 + (C \kappa \sigma_P)^2 + (C P \sigma_\kappa)^2} \quad (7)$$

239 where the uncertainties σ_P and σ_κ are standard deviations of averaged data from the measurement windows. The time series of flow rates and measured atmospheric pressure during the course of the experiment are shown in Figure 4.

241

242 Similarly, the uncertainty in the flow rate estimated by FAST method can be written as:

$$\sigma_{\hat{Q}} = \sqrt{(K_{FAST} \underline{C_{CL}} \sigma_{\underline{u_{CL}}})^2 + (K_{FAST} \underline{u_{CL}} \sigma_{\underline{C_{CL}}})^2 + (\underline{C_{CL}} \underline{u_{CL}} \sigma_{K_{FAST}})^2} \quad (8)$$

where $\sigma_{\underline{u_{CL}}}$ is the standard deviation of the wind speed in the downwind direction, $\sigma_{\underline{C_{CL}}}$ is the standard deviation of the

concentration measurements and $\sigma_{K_{FAST}}$ is the standard error in the estimate of K_{FAST} as shown in Figure 7 and Table 4.

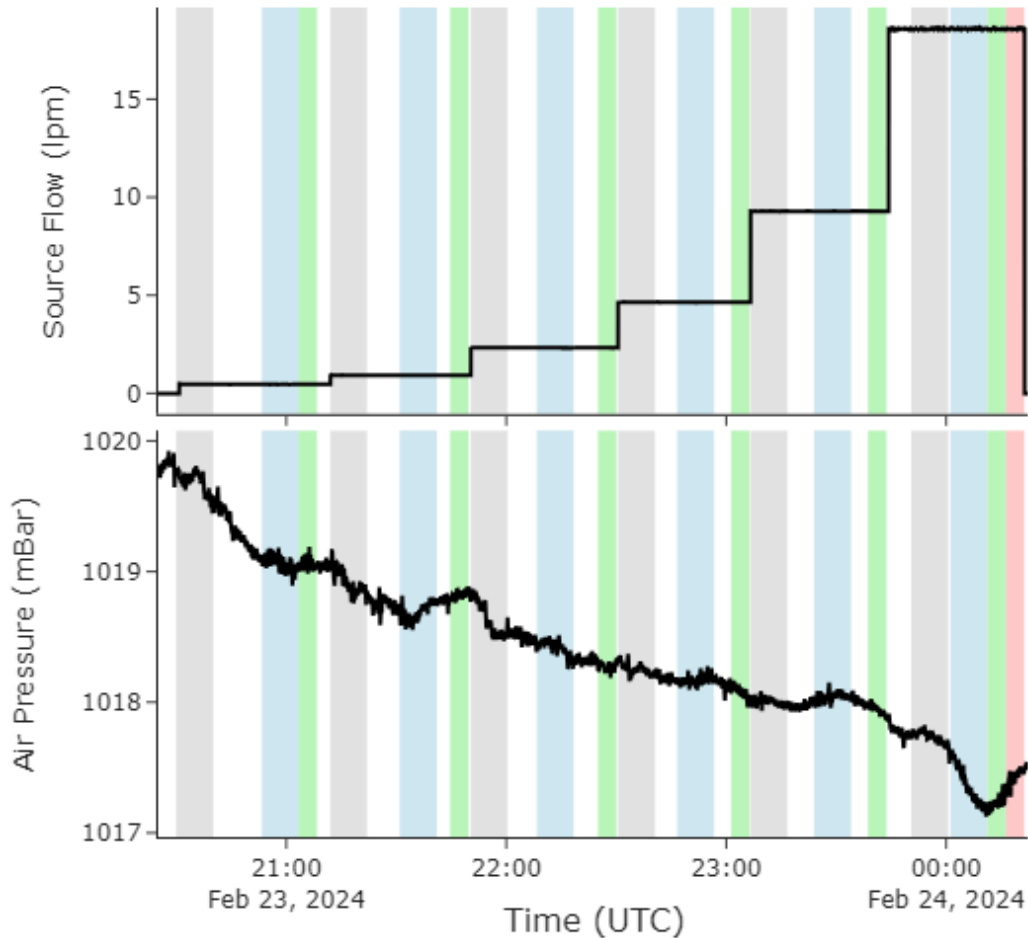


Figure 4: Time series of the output flow rate (liters per minute) throughout the Richmond controlled release experiment with shaded areas indicating the set measurement windows: gray for no fan state, blue for fan on at low speed, green for fan on at high speed, and red for maximum fan speed at the end of the experiment.

2.2.3 Data Filtering by Wind Direction

253 In order to optimize the FAST method under strong crosswind conditions, filtering was applied to improve data
 254 quality and estimate emissions more accurately. Despite the advection from the fan, strong crosswind interference introduces
 255 variability in both the concentration (C) and wind speed (u) measurements. Filtering addressed this issue by excluding data
 256 associated with wind directions unlikely to transport emissions directly to the sensors.

257 To filter the data, we first calculate the wind direction (Θ_i) from the x- and y-direction wind components (u and v) within a
 258 normalized range of [0, 360) degrees for each data point as follows:

$$259 \quad \Theta_i = ((\arctan2(v, u) * \frac{180}{\pi}) + 360) \bmod 360 \quad (9)$$

260 The mean wind direction, Θ_{mean} , is then computed as the arithmetic average of the normalized wind directions:

$$261 \quad \Theta_{mean} = \frac{1}{N} \sum_{i=1}^N \Theta_i \quad (10)$$

262 where N represents the total number of data points in a given measurement period.

263 We then apply a filter angle (ϕ) symmetrically around the mean wind direction to define the range of included data. The
 264 lower (Θ_{lower}) and upper (Θ_{upper}) bounds of the filtered range are defined as:

$$265 \quad \Theta_{lower} = (\Theta_{mean} - \frac{360 - \phi}{2}) \bmod 360 \quad (11)$$

$$266 \quad \Theta_{upper} = (\Theta_{mean} + \frac{360 - \phi}{2}) \bmod 360 \quad (12)$$

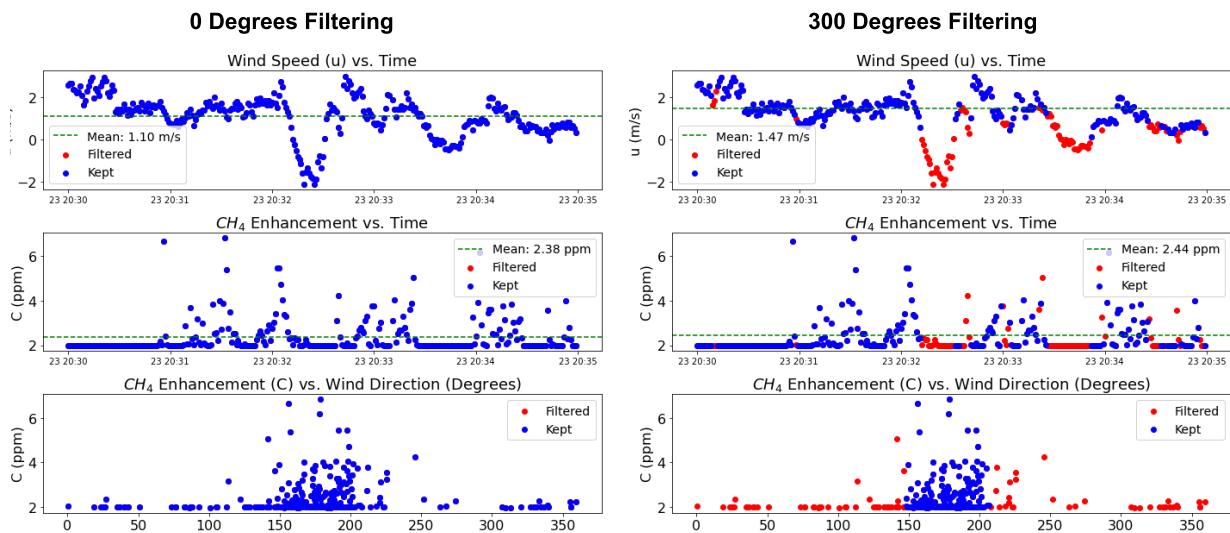
267 The wind and methane data are then filtered to include only directions within the specified range. If the bounds do not cross
 268 the 0 degree/360 degree discontinuity, the filtered data satisfies:

$$269 \quad \Theta_i > \Theta_{lower} \text{ and } \Theta_i < \Theta_{upper} \quad (13)$$

270 and when the bounds span the discontinuity, data satisfying the following conditions are used:

$$271 \quad \Theta_i > \Theta_{lower} \text{ or } \Theta_i < \Theta_{upper} \quad (14)$$

272 Figure 5 illustrates the impact of filtering on the time series of wind and methane concentration data, for a 1 g/hr
 273 release from the Richmond Field Station experiment (N = 300). As the filter angle decreases, more data from crosswind and
 274 background noise is excluded (shown in red) and the mean wind speed (u) and concentration (C) values change, resulting in
 275 different estimates from the FAST method. We found that a filter angle of 300° effectively aligns the analysis with wind
 276 directions closely aligned with the source when accounting for plume spread within $x < 2$ m.



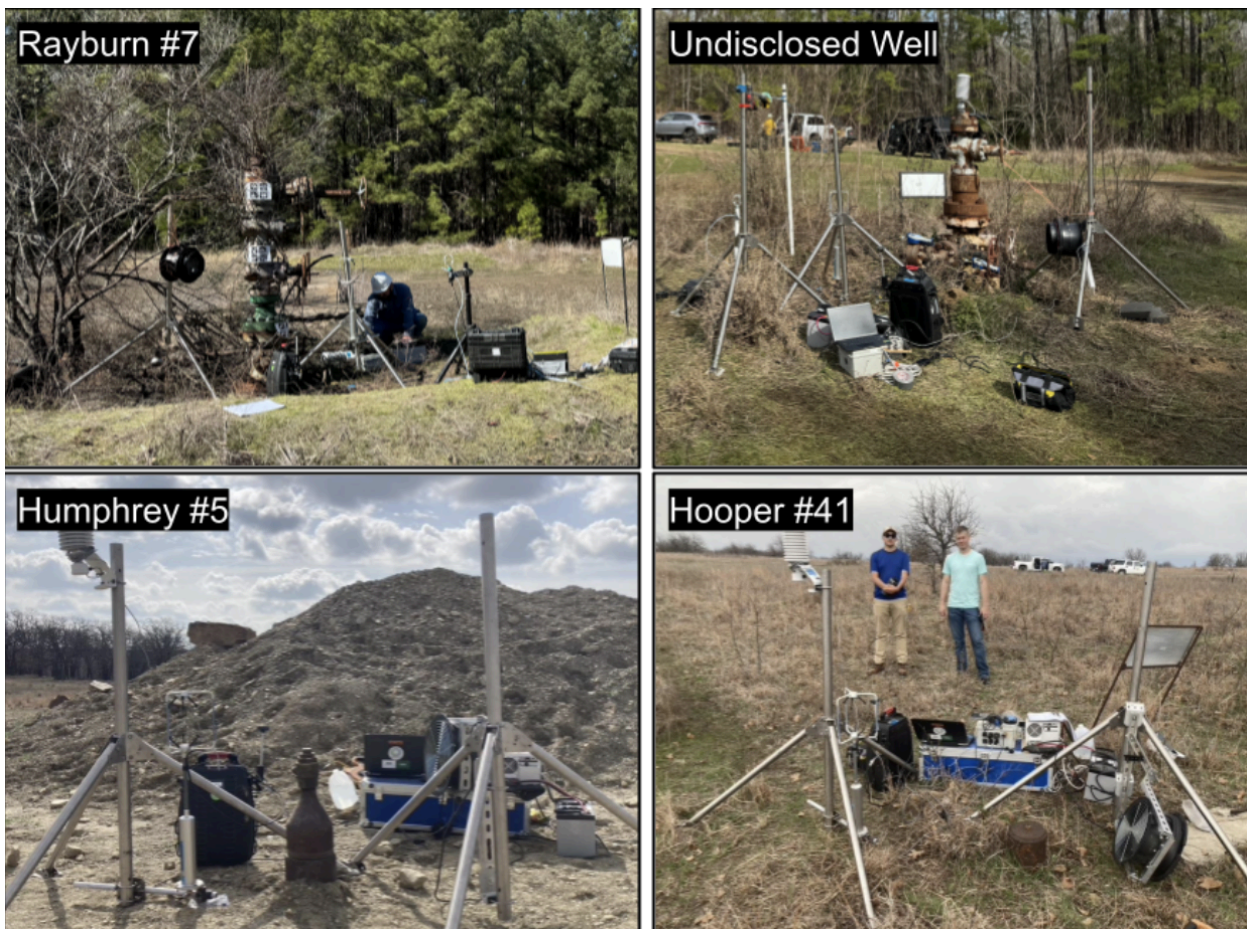
277
278 **Figure 5:** Time series of wind speed (u) and methane enhancement (C) as well as C vs. wind direction (in degrees) for a ‘no
279 fan’ release of 1 g/hr at the Richmond Field Station. Kept data are shown in blue while filtered data are shown in red. Mean
280 wind speed and concentration over the 5 minute measurement period are shown in green.

281

282 2.3 Field Experiments

283 The FAST method was tested on four wells during two field campaigns, two in Texas (6 and 7 February) and two in
284 Oklahoma (14 March), during the spring of 2024. For all field measurements, a similar setup was used to that in the
285 Richmond Field Station controlled release experiment. During the experiments in Texas, the background wind velocity was
286 < 1 m/s, so only the Low Fan setting was used for the two wells. In Oklahoma, background wind speeds were much higher
287 than those in Richmond, so both the Low Fan and High Fan settings were used. At each well, we measured background
288 (upwind) methane concentrations using the Picarro for five minutes and this background value was subtracted from the
289 methane concentrations collected during the FAST method to determine the enhancement. Figure 6 shows images of the four
290 wells discussed in the paper with the FAST method setup. For each well, SEMTECH and FAST measurements were taken;
291 FLIR measurements were taken in Texas only.

292



293
 294 **Figure 6:** Wells measured in Lufkin, Texas (top) and Barnsdall, Oklahoma (bottom) using the FAST method. Both wells in
 295 Texas were of the “christmas tree” variety (multiple potential leak points) and were measured using No Fan and Low Fan
 296 speeds because the background wind speeds were < 1 m/s. Both wells in Oklahoma were lower to the ground, had only one
 297 leak point and were measured with No Fan, Low Fan and High Fan speeds due to the higher background winds (> 1 m/s).
 298

299 3 Results

300 3.1 Fan Characterization Results

301
 302 Detailed results of the fan characterization experiments are provided in Appendix C. These experiments
 303 demonstrated that the High fan setting produced a more stable and uniform plume under higher background wind conditions,
 304 while the Low setting was sufficient for generating a stable plume in the absence of background wind. Wind speed
 305 measurements showed that the primary flow velocity decreased with downwind distance, reaching background levels beyond

approximately 2 meters. Analysis of the standard deviation of wind direction confirmed that plume dispersion followed a square-root dependence on distance for $x < 2$ meters, in agreement with theoretical expectations. Beyond this range, crosswind turbulence caused significant deviations from the expected dispersion behavior, leading to increased variability and instability in the plume structure. Additionally, measurements taken off the plume centerline ($y \neq 0$) exhibited greater variability due to crosswind effects, reinforcing the importance of positioning sensors along the centerline ($y = 0$) to ensure consistent and reproducible measurements. Based on these findings, all field experiments were conducted with sensors placed within 2 meters of the fan and along the centerline.

Furthermore, based on our fan experiments, we were able to estimate the parameters needed to calculate K_{FAST} using Equation 4. We measured the blade length of the MDB fan (l_{fan}) and estimated the turbulence intensity i_{fan} as the mean of the turbulence intensity measured in the first fan experiment during the High and Low fan settings for $x < 2$ m (see Figures C1 and C2). Using these values ($\beta = 1$, $i_{fan} = 0.23$, $l_{fan} = 0.13$ m, $x_0 = 2$ m), the effective K_{FAST} would be $K_{FAST} = \pi \beta i_{fan} l_{fan} x_0 = 0.19$ m², which matches the value determined during the controlled release experiment with maximum filtering (300 degrees).

3.2 Experimental Determination of K_{FAST}

Results from the Richmond Field Station controlled release experiment are summarized in Table 3. Using Equations 7 and 8, an estimate of the actual source rate (Q) was obtained which nearly matched the intended target rates of 1, 2, 5, 10, 20 and 40 g/hr. The SEMTECH HI-FLOW performed very well during the controlled release study, almost matching the exact values derived from stoichiometry. The FAST method estimates (generated using 10 minute averages and $K_{FAST} = 0.19$ m²) also match the source rate quite well, however with much larger uncertainties than the SEMTECH. Without the fan (No Fan), the FAST method tends to overestimate the lower range (1-5 g/hr) and severely underestimate the upper range (10-40 g/hr). This is greatly improved via the use of the fan, with the Low Fan setting performing slightly better in the upper range and the High Fan setting performing better in the lower range. These discrepancies could also be due to fluctuations in the background wind throughout the experiment which may have biased the results.

Source Rate $Q \pm \sigma_Q$ (g/hr CH ₄)	SEMTECH (g/hr CH ₄)	FAST (No Fan) (g/hr CH ₄)	FAST (Low Fan) (g/hr CH ₄)	FAST (High Fan) (g/hr CH ₄)
0.93 ± 0.03	0.96 ± 0.03	0.27 ± 2.94	0.65 ± 0.51	1.01 ± 0.50
1.86 ± 0.06	1.89 ± 0.05	1.34 ± 3.81	1.85 ± 1.17	2.81 ± 0.78
4.66 ± 0.17	4.62 ± 0.08	8.23 ± 16.14	3.65 ± 2.50	4.65 ± 2.38
9.33 ± 0.32	9.25 ± 0.16	2.40 ± 11.62	10.29 ± 4.99	9.75 ± 4.08
18.67 ± 0.63	18.30 ± 0.33	0.52 ± 2.01	16.74 ± 9.70	22.80 ± 7.14

37.32 ± 1.27	36.90 ± 0.53	32.54 ± 75.92	40.13 ± 21.70	38.20 ± 17.40
------------------	------------------	-------------------	-------------------	-------------------

Table 3: Comparison of the desired (target) and true (stoichiometric) release rate with those measured by the SEMTECH and FAST method (with 300 degrees of filtering) during the controlled release experiment at Richmond Field Station.

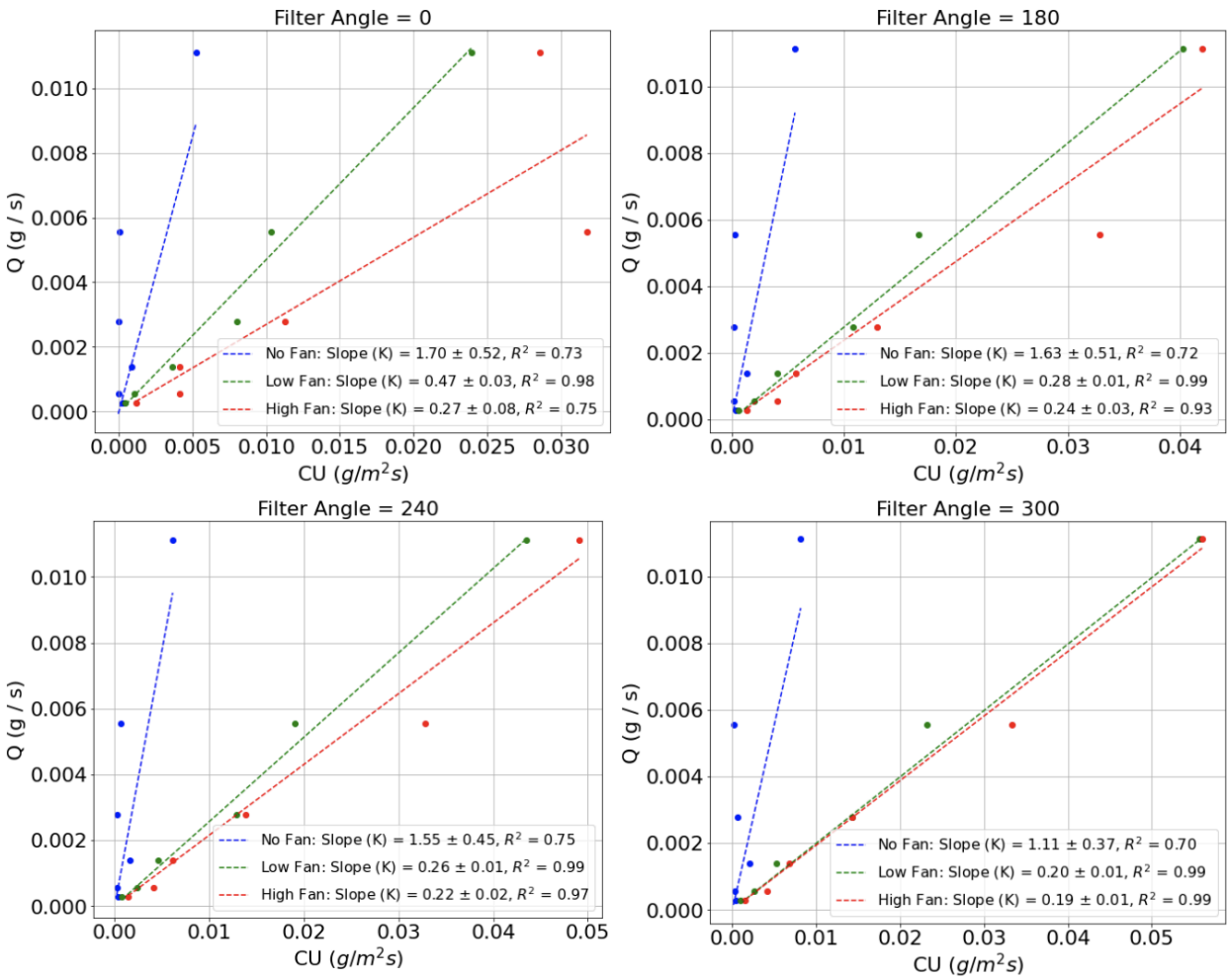


Figure 7: Measured mean $C * U$ (along x) vs. known Q (along y) for the control release experiment used to determine the values of K_{FAST} (slopes) for a range of fan speeds and filtering angles.

By using the known values of Q from stoichiometry (source rate) and the measured values of C and u during the controlled release experiment, the experimentally determined values of K_{FAST} for different filter angles and fan speeds are

348 estimated via Equation 3. By inverting Equation 3 to solve for K_{FAST} , $K_{FAST} = \frac{\overline{C_{CL}} \overline{u_{CL}}}{Q}$ where the known value of Q and 10
349 minute averages of C_{CL} and u_{CL} are used to estimate K_{FAST} . The resulting values for K_{FAST} are shown as the slopes of the lines
350 in Figure 7 along with the uncertainties resulting from standard error estimates on the linear regression used to generate the
351 line of best fit. As expected, the No Fan scenario has a much higher value of K_{FAST} with higher overall uncertainty due to the
352 variation of the natural wind direction and speed. Without filtering the data by wind direction, the K_{FAST} values are larger
353 (likely due to more dispersion from crosswinds). Furthermore, K_{FAST} values at the low and high fan speeds do not agree,
354 although K_{FAST} is theoretically independent of fan speed (per Equation 4). As more and more crosswind is filtered (Filter
355 Angle approaches 360 degrees), the low and high fan speeds converge to a K_{FAST} of around 0.19 m^2 , as expected. All fits are
356 done with a 0 intercept and standard errors are used to estimate the uncertainty of K_{FAST} . Table 4 shows the resulting
357 experimentally determined values of K_{FAST} and their corresponding uncertainties which were used to estimate emissions and
358 corresponding uncertainties from field measurements.

359

Filter Angle	No Fan	Low Fan	High Fan
0 Degrees	1.70 ± 0.52	0.47 ± 0.03	0.27 ± 0.08
180 Degrees	1.63 ± 0.51	0.28 ± 0.01	0.24 ± 0.03
300 Degrees	1.11 ± 0.37	0.20 ± 0.01	0.19 ± 0.01

360 **Table 4:** Values of K_{FAST} in m^2 and their associated uncertainties under various filter and fan conditions determined from the
361 Richmond controlled release experiment.

362

363 3.3 Field Campaigns

364

365 3.3.1 Texas Field Campaign

366

367 The first field campaign that measured orphaned wells using the FAST method took place in February 2024 in
368 collaboration with multiple agencies. The U.S. Forest Service (USFS) invited the U.S. Department of Energy's Consortium
369 Advancing Technology for Assessment of Lost Oil and Gas Wells (CATALOG) team to help measure and assess emissions
370 from certain wells being plugged using funds from the Infrastructure Investment and Jobs Act (IIJA). The FAST method was
371 deployed in the field campaign to understand emission patterns better and help allocate sealing funds more efficiently.

372

373

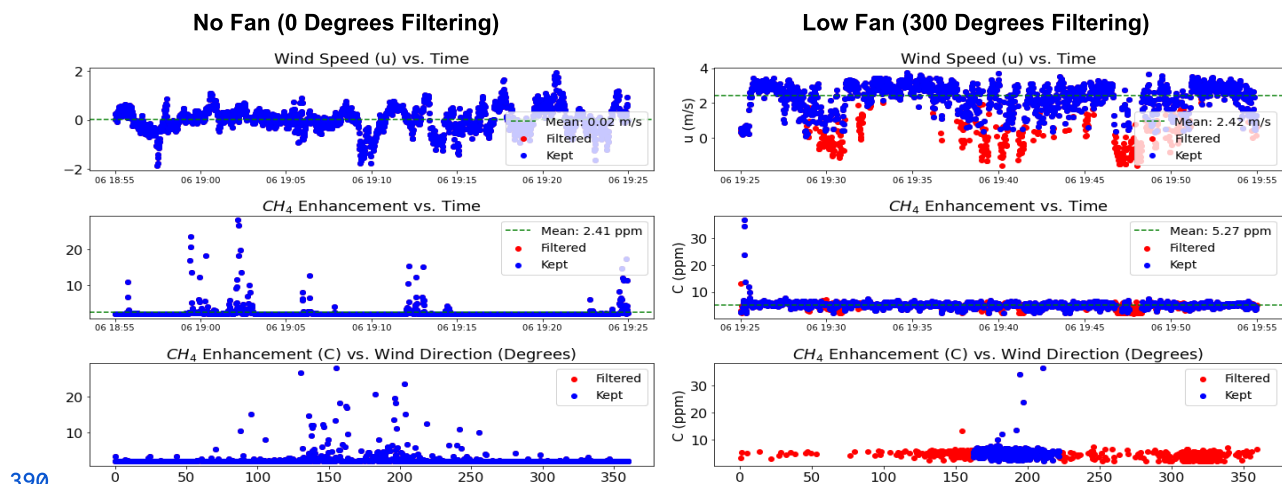
374 Rayburn #7

375

376 Rayburn #7 is an oil production well identified by API number 4200530245 and associated with district/lease
377 number 06/13688. Its geographical coordinates are 31.0865, -94.1974, and its total depth is 12,927 feet. On February 6, 2024
378 during the initial detection of Rayburn #7, a small leak was found from a threaded port on a valve junction 1.2 meters above
379 the ground by sniffing the casing of the well with the Picarro G4302. The well is situated in a large clearing with a gravel
380 pad and other infrastructure, surrounded by an embankment. A plastic spill tub and several 500-gallon drums were observed
381 close to the wellhead. Furthermore, a compressor station and separation/storage infrastructure are located in the corner of the
382 clearing. No leak was detected on any of the other infrastructure in the area. A Gill R3-50 sonic anemometer was placed at

the height of 1.2 meters and 0.94 meters away from the methane source, alongside with the inlet to the Picarro G4302 methane detector. Sampling commenced at 12:20 under ambient conditions for 60 minutes. The background methane concentration was 2.11 ppm. Following this, there were two more sets of sampling periods: 30 minutes each for ambient conditions and low fan conditions. The SEMTECH measured an emission rate of 2.86 grams per hour, with a standard deviation during the averaging period of $\pm 0.04\text{g/h}$ (Figure B2a). The FLIR camera could not provide a clear visual indication of the leak.

389



390

Figure 8: Time series of wind speed (u) and methane enhancement (C) as well as C vs. wind direction (in degrees) for ‘no fan’ setting from a ‘low fan’ setting. Kept data are shown in blue while filtered data are shown in red. Mean wind speed and concentration over the 30 minute measurement periods are shown in green.

Figure 8 illustrates the effect of using the fan on the time series of concentration and wind speed measurements at Rayburn #7, providing insight into the variability of methane concentrations and plume enhancements. Without the fan (Figure 8, left), the average wind speed in the x-direction (u) over the 30-minute measuring period was approximately 0 m/s. However, infrequent gusts in the x-direction caused spikes in methane concentrations, ranging from about 10 to 20 ppm above background levels. These spikes were spread across a wide range of directions, between 100 and 250 degrees, indicating variable plume dispersion under stagnant conditions. With the fan on at a low setting (Figure 8, right), the mean wind speed in the x-direction (u) increased to approximately 2 m/s, and the plume became more stable. The methane concentration spikes were more concentrated in direction, between 180 and 210 degrees, corresponding to the airflow from the fan. While a large spike was observed at the start of the low fan measurement, likely due to the fan turning on, the concentration stabilized to around 5 ppm above background levels after this initial adjustment.

Undisclosed Well

405

The methane emission detection and monitoring experiment at this undisclosed location identified two leak points on one wellhead. The FLIR did not detect any emissions from either of the leak sources. There was a small leak at the end of a main pipe flange and a more significant leak in a connection thread on the same flange, which was the primary point source. The FAST system was set up at 11:45 UTC on February 7, 2024, pointed at 315 degrees N, with the fan turned off. The fan was located 58 cm above the ground and 87 cm upwind from the source, which is within the range of <1 m. The

411 Gill R3-50 sonic anemometer and Picarro G4302 gas analyzer inlets were positioned 73 and 71 cm above the ground and 97
412 and 95 cm horizontally from the source, respectively. The primary source was at a height of 47 cm. The background methane
413 concentration was 2.08 ppm. The experiment with the fan turned on started at 13:22 UTC. Data was collected for two
414 15-minute periods with the fan on and two 15-minute periods with the fan off. Analogous to the Rayburn #7 experiment, the
415 anemometer orientation was set in a manner that 0 degrees represents the direction where it is facing the upwind source and
416 fan line. For this experiment, wind direction had favorable conditions, which led to significant data acquisition for the
417 periods without the fan. The SEMTECH measured an emission rate of 0.95 grams per hour, with a standard deviation during
418 the averaging period of ± 0.25 g/h (Figure B2b).

419

420

421 3.3.2. Oklahoma Field Campaign

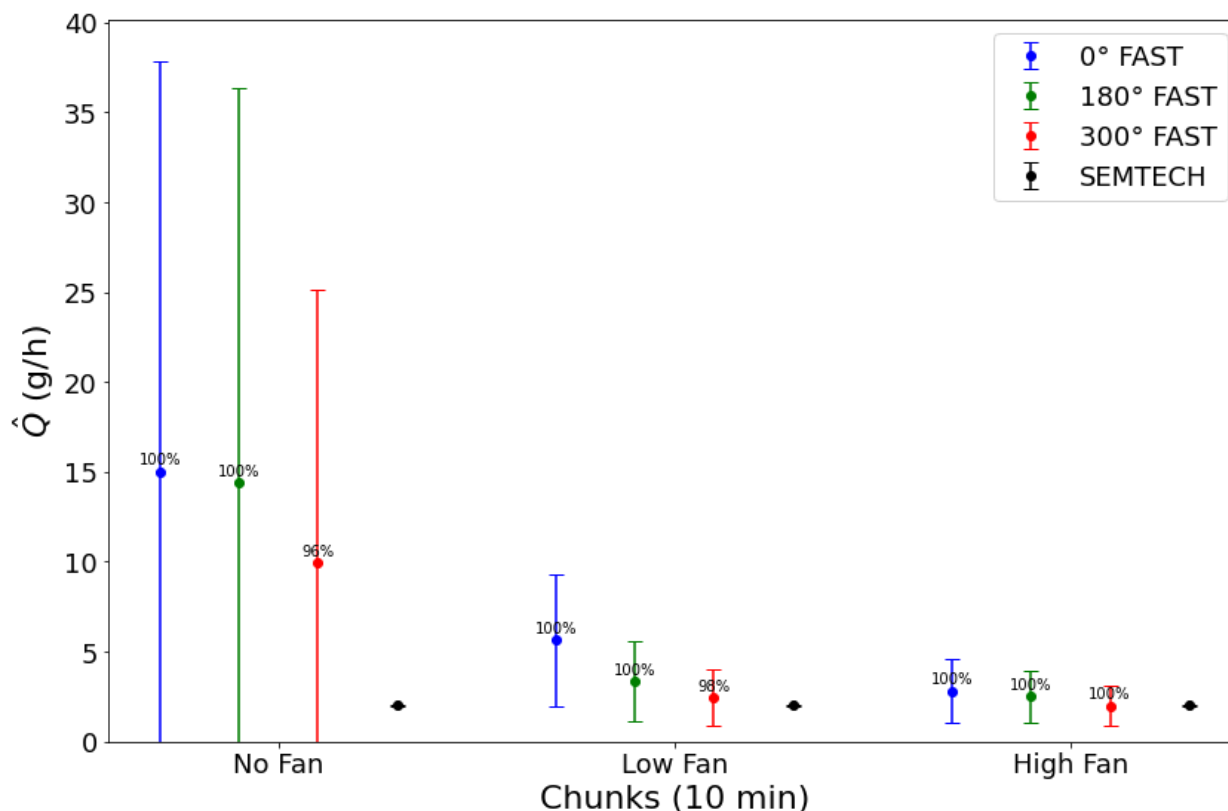
422

423 Humphrey #5

424

425 Humphrey #5 is an orphaned well that was located by our team during surveying on March 14th, 2024. The FAST
426 method was set up and measured for 10 minutes at each fan speed (No, Low, High) as shown in Figure 9. The leak was from
427 the top cap of the well head at a height of 0.62 m, and the sensors were positioned downwind at 0.4 m from the leak and a
428 height of 0.65 m. The fan was set up at a height of 0.6 m and an angle of 5 degrees upward (to generate a plume that passed
429 through the anemometer) at 0.5 m upwind of the well. The SEMTECH measured an emission rate of 2.03 grams per hour,
430 with a standard deviation during the averaging period of ± 0.04 g/h (Figure B2c).

431



432

433 **Figure 9:** Estimated leak rates (\hat{Q}) and uncertainties ($\sigma_{\hat{Q}}$) from FAST method measured in 10 minute increments (colored)
 434 and SEMTECH (black) for Humphrey #5, labeled by percentage of data kept after filtering. For the “No Fan” setting (left
 435 most), the estimate is very uncertain and much higher than the SEMTECH.

436

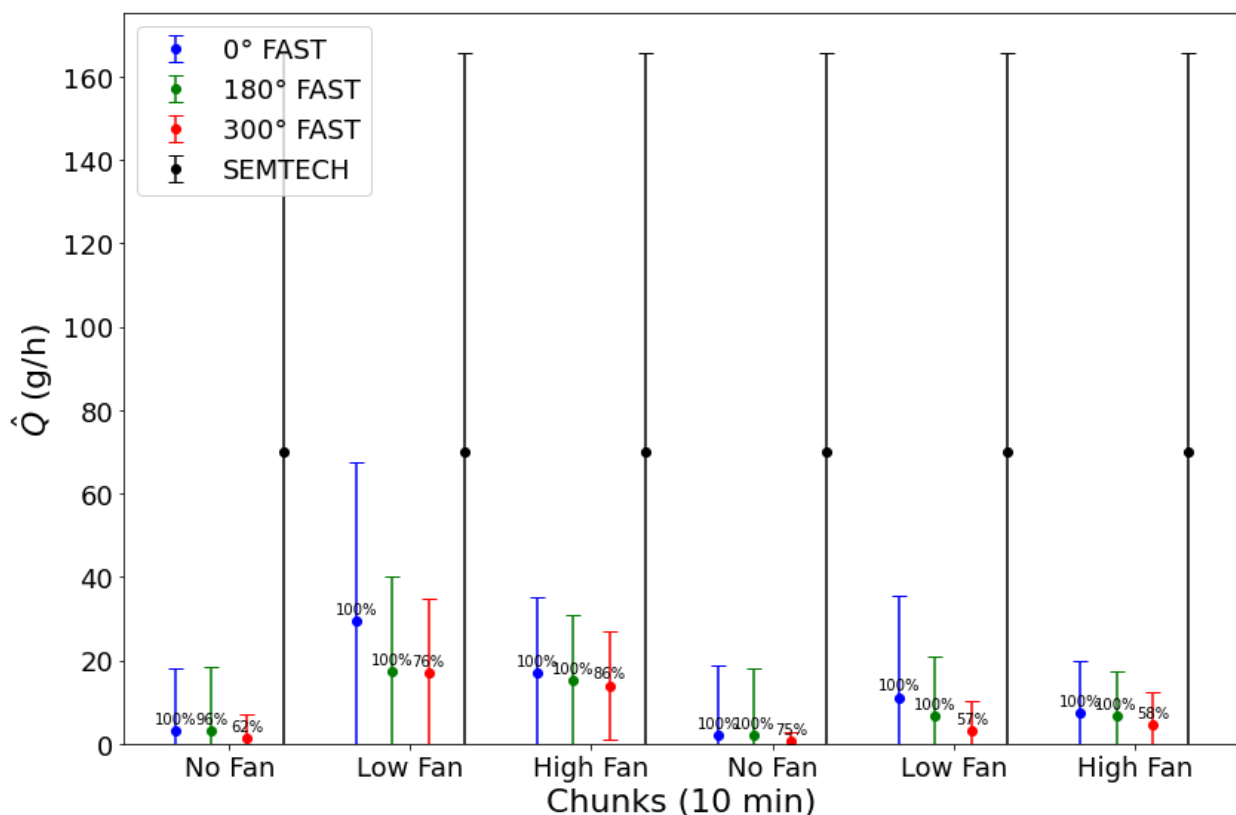
437

438 Hooper #41

439

440 Hooper #41 is another UOW that was also discovered by the team on March 14th, 2024 near Barnsdall, OK. The
 441 leak was from the top cap of the well head at a height of 0.25 m, the sensors were positioned downwind at 0.88 m from the
 442 leak and a height of 0.65 m. The fan was set up at a height of 0.27 m and an angle of 24 degrees upward at 0.4 m upwind of
 443 the well. Interestingly, this well seemed to have a variable leak rate, resulting in a very high uncertainty on the SEMTECH.
 444 The SEMTECH measured an intermittent averaged emission rate of 70.14 g/h, with a large standard deviation during the
 445 averaging period of ± 95.47 g/h (Figure B2d). The FAST method was used in 10 minute intervals for No, Low, and High fan
 446 settings. Due to the highly variable nature of the well, these measurements were repeated in the same intervals for
 447 comparison (Figure 10). During both measurement periods, the FAST method estimates the well to only emit around 10 +/-
 448 10 g/h as opposed to 70 +/- 90, which the SEMTECH reported.

449



450

451 **Figure 10:** Estimated leak rates (\hat{Q}) and uncertainties ($\sigma_{\hat{Q}}$) from FAST method measured in 10 minute increments (colored)
 452 and SEMTECH (black) for Hooper #41, labeled by percentage of data kept after filtering. Due to the high variability of the
 453 well, it was measured twice with the FAST method at 10 minute increments (sequentially). Here, the SEMTECH did not get
 454 a good reading due to the instability in the CH_4 concentration of the sampling volume.

455 The results for Hooper #41 highlight challenges in measuring methane emissions from variable wells and suggest
 456 potential limitations in the FAST method. The variable leak rate led to significant uncertainty in SEMTECH readings
 457 (± 95.47 g/h), while the FAST method provided more stable estimates (10 ± 10 g/h). However, the fan setup likely failed to
 458 fully entrain the emitted gas into the airflow directed toward the sensor, potentially leading to an underestimation of
 459 emissions, as supported by SEMTECH data and Figure 10. This limitation is particularly critical for wells with low-height
 460 emissions, such as Hooper #41. Future work could address this limitation through controlled release experiments at different
 461 heights to optimize the fan and sensor configurations for capturing low-lying plumes.

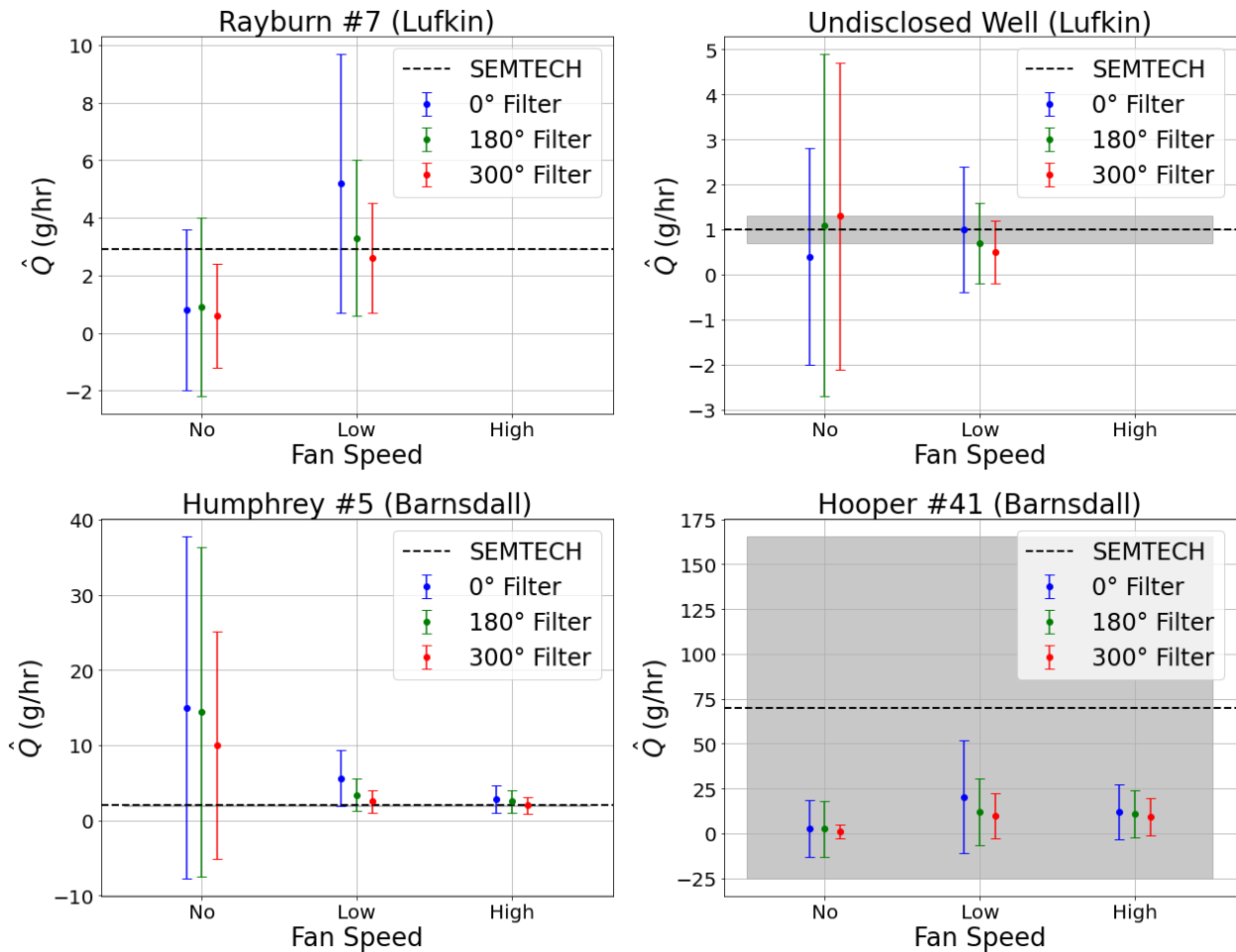
462

463 4. Discussion

464

465 The results of the field campaigns are summarized in Table 5 and Figure 11. For each of the four wells measured,
 466 the FAST method results are based on 10 minute averages and K_{FAST} values corresponding to the fan speed and various levels
 467 of filtering (0, 180 and 300 degrees) as shown in Figure 7 and Table 4. The uncertainty in the FAST estimates is calculated

468 using Equation 8. Overall, the FAST method agrees with the SEMTECH for both the Low and High fan settings but not for
469 the No Fan settings. These uncertainties decrease with a larger filtering angle and a higher fan speed. Furthermore, emission
470 rate estimates for all four wells were calculated using a Gaussian Plume Model (GPM) and described in Appendix A for
471 comparison.
472

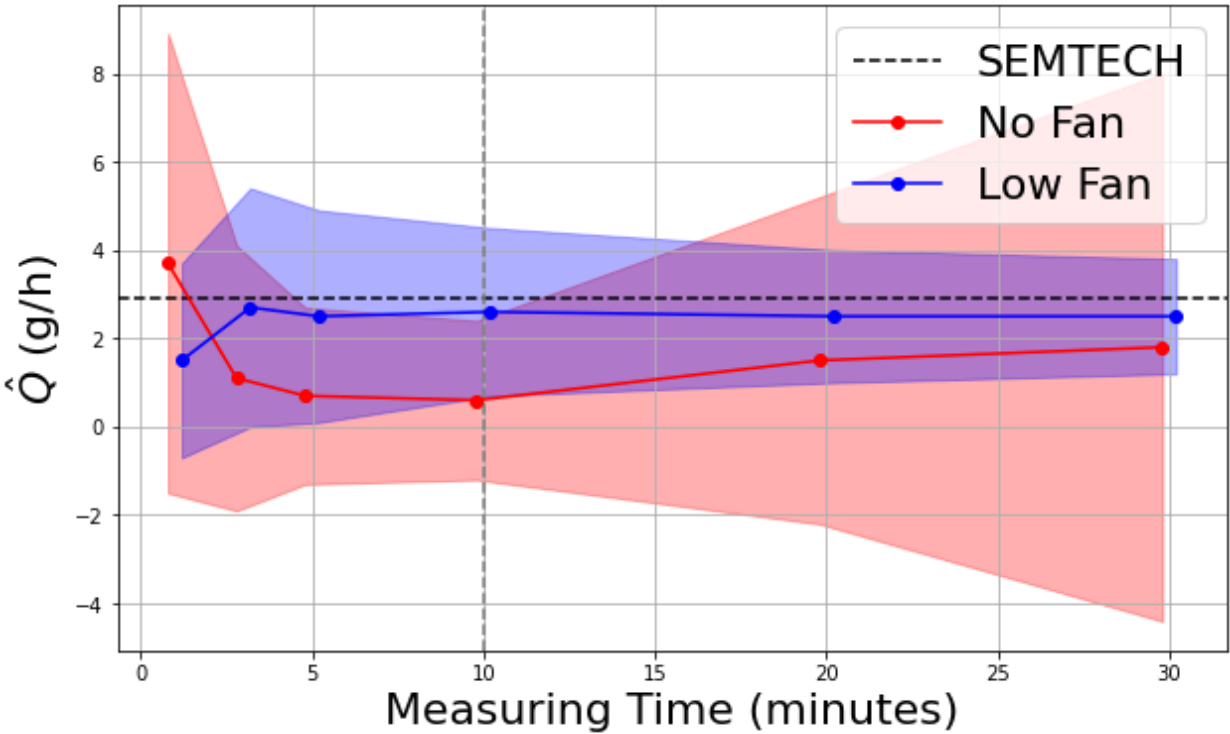


473
474 **Figure 11:** Estimated leak rates (\hat{Q}) and uncertainties ($\sigma_{\hat{Q}}$) for the four wells shown in Figure 6 from the SEMTECH (black
475 and gray) and FAST method (colored). SEMTECH is able to get very accurate readings for all wells except Hooper #41
476 which was a highly variable well.
477
478

Date	Well ID	SEMTECH (g/hr)	FAST (0 Filter) (g/hr)	FAST (180 Filter) (g/hr)	FAST (300 Filter) (g/hr)

2024-02-06	Rayburn #7 (Lufkin)	2.9 ± 0.0	Low: 5.2 ± 4.5 No: 0.8 ± 2.8	Low: 3.3 ± 2.7 No: 0.9 ± 3.1	Low: 2.6 ± 1.9 No: 0.6 ± 1.8
2024-02-07	Undisclosed Well (Lufkin)	1.0 ± 0.3	Low: 1.0 ± 1.4 No: 0.4 ± 2.4	Low: 0.7 ± 0.9 No: 1.1 ± 3.8	Low: 0.5 ± 0.7 No: 1.3 ± 3.4
2024-03-14	Humphrey #5 (Barnsdall)	2.0 ± 0.04	High: 2.8 ± 1.8 Low: 5.6 ± 3.7 No: 15.0 ± 22.8	High: 2.5 ± 1.5 Low: 3.4 ± 2.2 No: 14.4 ± 21.9	High: 2.0 ± 1.1 Low: 2.5 ± 1.5 No: 10.0 ± 15.1
2024-03-14	Hooper #41 (Barnsdall)	70.1 ± 95.5	High: 12.1 ± 15.3 Low: 20.2 ± 31.4 No: 2.6 ± 15.8	High: 10.8 ± 13.3 Low: 12.0 ± 18.6 No: 2.6 ± 15.6	High: 9.3 ± 10.4 Low: 9.9 ± 12.7 No: 1.0 ± 4.0

479 **Table 5:** Estimated leak rates (\hat{Q}) and uncertainties ($\sigma_{\hat{Q}}$) for the four wells shown in Figure 6 from the SEMTECH and FAST
 480 method. SEMTECH is able to get very accurate readings for all wells except Hooper #41 which was a highly variable well.
 481



482
 483 **Figure 12:** Estimated leak rates (\hat{Q}) and uncertainties ($\sigma_{\hat{Q}}$) from the FAST method for Rayburn #7 as a function of the
 484 sampling time used to make the estimate. Without a fan, the measurement is highly uncertain throughout, except for the

range from 5-10 minutes. With the fan, the measurement accuracy gets higher with increasing measurement time, but the mean value stays roughly constant above 3 minutes. This shows that the FAST method can be done as quickly as the SEMTECH and accuracy only increases with increased measuring time.

Figure 12 shows the results of the FAST method at the Low fan (blue) and No fan (red) settings on Rayburn #7, which was measured in 30 minute intervals, as well as the SEMTECH estimate (black dashed line). For the Low fan setting, the SEMTECH value is always within the uncertainty of the FAST method, even if only the first minute of data is used. The mean rate improves when the measuring time is increased to three minutes, but the error bars remain large. For measuring times larger than three minutes, the error bars decrease nearly linearly with increased measuring time, while the mean stays relatively constant. The No Fan results, on the other hand, do not match the SEMTECH well for measuring time shorter than 10 minutes. As expected, as the measuring time increases, the mean value of the FAST method for No Fan gradually approaches the SEMTECH, but the error bars also increase over time. This shows that the measuring time for the FAST method, even at the Low Fan measurement, is similar to that of the SEMTECH (on the order of 3 minutes).

The total cost of the sensors used in this study, a Picarro G4302 for concentration (~40,000 USD) and Gill Windmaster 1210-PK-085 (~5,000 USD) for wind, are about the same cost as a SEMTECH HI-FLOW (~50,000 USD). However, the FAST method can be done without using 3D wind measurements. By replacing the 3D anemometer with a 1D anemometer, the cost of the FAST method can be decreased with minimal loss in accuracy. Effectively, using a 1D anemometer would limit the filter angle to be up to 180 degrees, which has marginally worse accuracy than filtering by 300 degrees. Furthermore, the type of methane sensor can be optimized to a more reasonable price point, as CH₄ signals near sources are typically high (e.g., > 1 ppm for leaks > 1 g/h). Future work will focus on investigating a wide variety of methane detection technologies to identify more cost-effective and reliable solutions for wide-scale FAST method deployment.

Besides its potential for being lower cost, the FAST method has other advantages over the existing technologies we tested (FLIR and SEMTECH). First, the FLIR camera is insensitive to small leaks and unable to detect most diffuse emissions and is unable to quantify emissions accurately [Zeng and Morris, 2019]. Furthermore, while our existing proof-of-concept FAST hardware is currently heavier and more complex to operate than a SEMTECH, it could be replicated with a battery powered fan mounted to a tripod or a backpack vacuum blower, making it very similar to the size and labor requirements of the SEMTECH. Although both the FAST method and the SEMTECH take approximately three minutes to obtain a measurement, the FAST method currently requires a longer setup time (~30 minutes) compared to the SEMTECH (~5 minutes).

5. Conclusions

We have shown that using a fan to create a forced flow at close range between the emission source and a point methane (CH₄) sensor and measuring 3D wind profiles using a sonic anemometer and CH₄ concentration with a gas analyzer (sampling technique), a simple estimate of the CH₄ emission rate of the source can be inferred (FAST method). The FAST method has been tuned using single, continuous point sources between 0.9 and 37 g/h at 1 m above the ground, in a simple aerodynamic landscape (grass field), in moderate meteorological conditions (< 5 m/s). Under these conditions, the FAST method consistently provided reasonable estimates of leak rates when fan speeds and filtering were applied appropriately, performing similarly to the commercially available method (SEMTECH) and outperforming others (FLIR). Notably, the method's performance improves with increased fan speed and filtering angle. For instance, in the case of Rayburn #7 in Lufkin, Texas, the FAST method at the Low Fan speed consistently produced leak rate estimates that were within the

529 uncertainty bounds of the SEMTECH values after just a few minutes of measurement. Without the use of a fan, the results
530 showed much greater uncertainty, highlighting the importance of airflow in stabilizing methane dispersion for accurate
531 estimation.
532

533 In the Texas and Oklahoma field campaigns, the FAST method provided accurate and rapid readings under varying
534 environmental conditions, with errors on the order of 95% of the emission rate across different wind conditions and leak
535 rates. In Texas, where wind speeds were low, only the Low Fan setting was used, and FAST results aligned closely with
536 SEMTECH, within 10%. In Oklahoma, higher wind conditions required both Low and High Fan settings to account for
537 greater natural dispersion. At Hooper #41, where emission rates fluctuated significantly, FAST produced lower overall
538 estimates than SEMTECH, likely due to its larger sampling cross-section averaging out short-term variability. However,
539 fan-driven airflow may not fully entrain all emitted gas, particularly from low-height leaks, which could contribute to an
540 underestimation of emission rates in certain cases.

541 The FAST method offers a potential alternative to existing technologies such as SEMTECH and FLIR for
542 identifying high-priority orphan wells. Its combination of controlled airflow and real-time methane measurement enables
543 rapid assessments suitable for large-scale monitoring. Ongoing research aims to refine wind and methane sensor integration
544 to improve cost efficiency while maintaining measurement accuracy across diverse field conditions and leak rates.

545

546 **Appendix A: Comparison to Gaussian Plume Method**

547 The approach to deriving the equations governing the FAST method outlined in the “Mathematical Model” section
548 can also be compared to the more traditional approach using a Gaussian Plume model (GPM). Through this comparison, we
549 can gain deeper insight into the physical significance of the proportionality constant (β), as it relates to the diffusivity of the
550 pollutant of interest. Including a term for reflection from the ground (but not from an inversion aloft), the GPM estimates the
551 downwind concentration of a pollutant as a function of the emission rate (Q), advective velocity (u), crosswind distance from
552 centerline (y), vertical displacement from centerline (z), height of the emission source (H) and horizontal and vertical
553 dispersion coefficients ($\sigma_y \sigma_z$) as follows:

$$554 \quad C(x, y, z) = \frac{Q}{2\pi \sigma_y \sigma_z u} \exp\left\{-\frac{y^2}{2\sigma_y^2}\right\} \left(\exp\left\{-\frac{(z-H)^2}{2\sigma_z^2}\right\} + \exp\left\{-\frac{(z+H)^2}{2\sigma_z^2}\right\} \right) \quad (A1)$$

555

556 Similar to the FAST model, the GPM assumes that the velocity profile is constant in space. However, the GPM does
557 not assume the concentration profile is constant, which is implicitly done by the FAST method via the use of centerline
558 time-averaged concentrations (Figure A1). Rather, the GPM assumes that the concentration profiles are Gaussian in the y
559 and z directions, with standard deviations (σ_y, σ_z) related to the width of the plume. These standard deviations are often
560 approximated using empirical data (i.e. Pasquill stability classes) but can be defined exactly using the diffusivity of the
561 pollutant (D). Assuming that the plume is isotropic and homogeneous, we can define:

$$\sigma_y \approx \sigma_z \approx \hat{\sigma} = \sqrt{\frac{2Dx}{u}} \quad (A2)$$

where D is the diffusivity of the pollutant and $\hat{\sigma}$ is the standard deviation of the Gaussian plume in all directions orthogonal to x. Evaluating this equation at some downwind distance x_0 and substituting our earlier use of centerline velocity measurements (given that the velocity profile is assumed constant in both GPM and FAST), we can define the standard deviation there ($\hat{\sigma}_0$):

$$\hat{\sigma}_0 \approx \sqrt{\frac{2Dx_0}{u_{CL}}} \quad (A3)$$

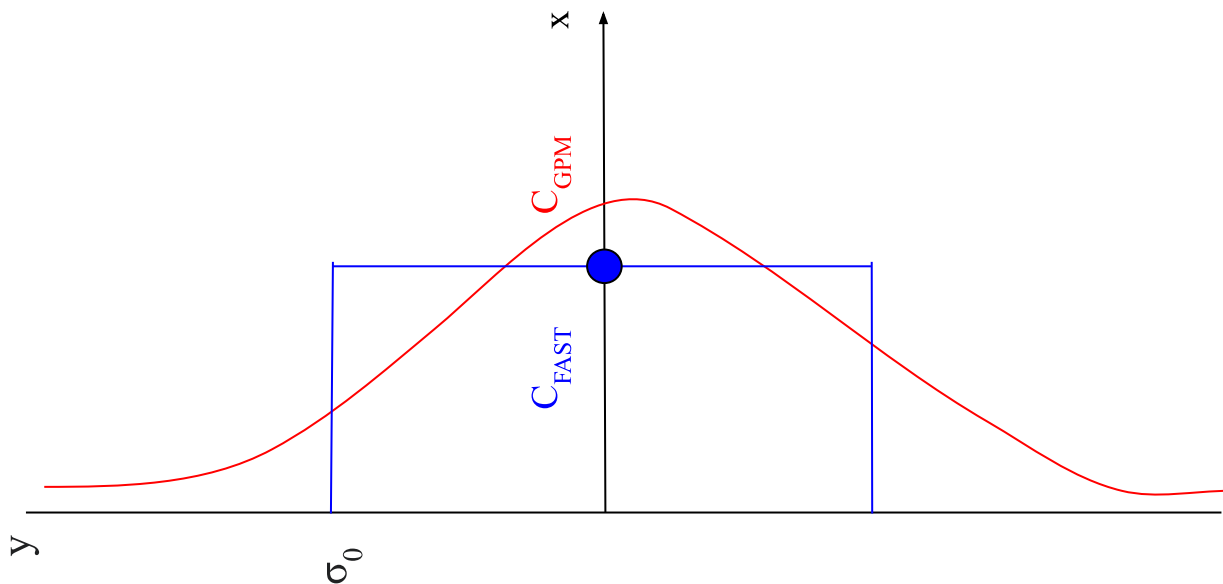
Using this standard deviation, we can imagine integrating the FAST approach over a certain number of standard deviations to capture more and more of the true concentration profile. To capture 99.7% of the total plume, we would need to integrate out to three standard deviations, or $3\hat{\sigma}_0$. Using this comparison to the previous equation derived for FAST (Equation 2), we can solve for β .

$$\sigma_0 = \sqrt{\beta i_{fan} l_{fan} x_0} \approx 3\hat{\sigma}_0 \approx 3 \sqrt{\frac{2Dx_0}{u_{CL}}}$$

(A4)

$$\beta \approx \frac{18 D}{i_{fan} l_{fan} u_{CL}} \quad (A5)$$

Here, we find that the proportionality constant β can be understood as a non-dimensional ratio of two diffusivities - one being the true diffusivity of the gas and the other being due to the turbulence generated by the fan. Since D can be very difficult to measure, the FAST method provides a work-around such that only constants related to the fan-generated flow need to be defined to quantify the emission rate. Equation A5 could also be inverted to estimate the diffusivity D, but this is not of real interest for this study



585

586

587 **Figure A1:** Diagram showing the difference in concentration profiles (C) used by the FAST (blue) and GPM (red) methods

588

589 We also calculated the estimated emissions from a Gaussian Plume Model (GPM) using three different Pasquill
590 Stability Classes (A, B and C) based on the no fan concentration and wind measurements for each well (shown in the table
591 below). As evidenced by the order of magnitude range for each well, the GPM is highly sensitive to the choice of stability
592 class, which is not immediately apparent for such short range measurements. We used the equations for calculating σ_y and
593 σ_z from [Cooper and Alley, 2011, pp. 662-663].

594

Date	Well ID	SEMTECH (g/hr)	FAST (300 Filter) (g/hr)	GPM for Daytime Pasquill Stability Classes (g/hr)
2024-02-06	Rayburn #7 (Lufkin)	2.9 ± 0.0	Low: 2.6 ± 1.9 No: 0.6 ± 1.8	Class A: 3.41 ± 20.2 Class B: 0.87 ± 5.18 Class C: 0.01 ± 0.08
2024-02-07	Undisclosed Well (Lufkin)	1.0 ± 0.3	Low: 0.5 ± 0.7 No: 1.3 ± 3.4	Class A: 1.05 ± 13.5 Class B: 0.27 ± 3.45 Class C: 0.0 ± 0.0

2024-03-14	Humphrey #5 (Barnsdall)	2.0 ± 0.04	High: 2.0 ± 1.1 Low: 2.5 ± 1.5 No: 10.0 ± 15.1	Class A: 226 ± 336 Class B: 57.8 ± 85.8 Class C: 1.06 ± 1.57
2024-03-14	Hooper #41 (Barnsdall)	70.1 ± 95.5	High: 9.3 ± 10.4 Low: 9.9 ± 12.7 No: 1.0 ± 4.0	Class A: 70.0 ± 332 Class B: 17.8 ± 84.2 Class C: 0.0 ± 0.0

Table A1: Estimated leak rates (\hat{Q}) and uncertainties ($\sigma_{\hat{Q}}$) for the four wells shown in Figure 6 from the SEMTECH, FAST method (filtered) and a Gaussian Plume Model (GPM) for all possible daytime Pasquill Stability Classes.

Based on there being moderate to strong insolation and low wind speeds (<2 m/s) for the Texas wells, the most likely stability class for Rayburn #7 and Undisclosed Well is Class A or B. Using these stability classes, the GPM does reasonably well at estimating the magnitude of the leak but the uncertainty is much higher than both the SEMTECH and the FAST method. Due to the higher background wind speeds (3-5 m/s) and moderate to strong insolation in Oklahoma, the B and C stability classes are most likely for Humphrey #5 and Hooper #41. Here, the GPM overestimates the magnitude of Humphrey #5 by orders of magnitude and the uncertainty is very high. For Hooper #41, which is a highly variable well, the GPM also still performs poorly relative to the SEMTECH and FAST methods.

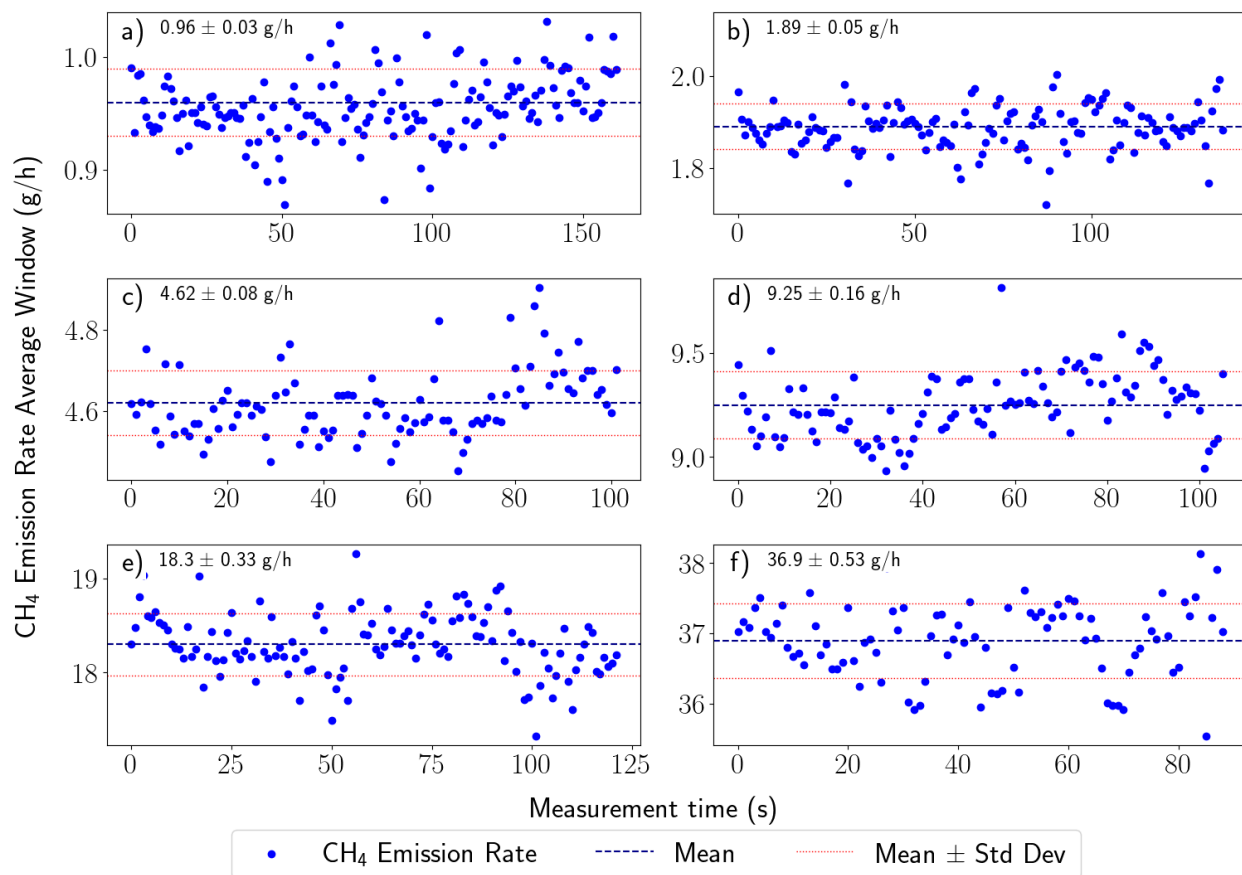
Appendix B: SEMTECH Measurements

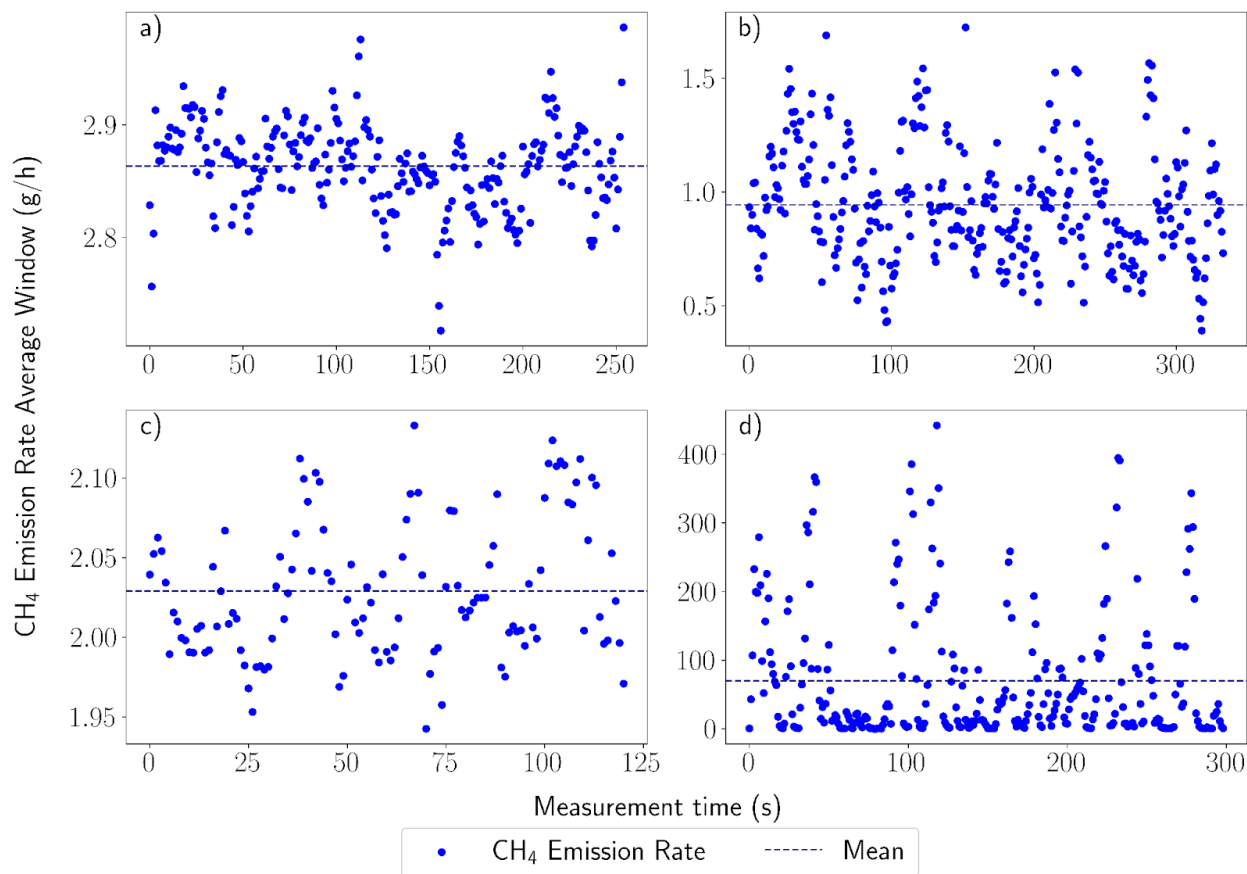
The SEMTECH Hi-Flow 2 is a methane emission quantification system composed of a backpack-mounted gas analyzer and a long sampling inlet tube with a fan to sample the methane emitted by a point source. This system reports the flow of methane emitted in liters per minute (LPM) in a range of 0.02 LPM to 730 LPM (1 g/hour - 29 kg/hour) (0.001 CFM to ~25 CFM), with an accuracy of ~10% [SEMTECH].

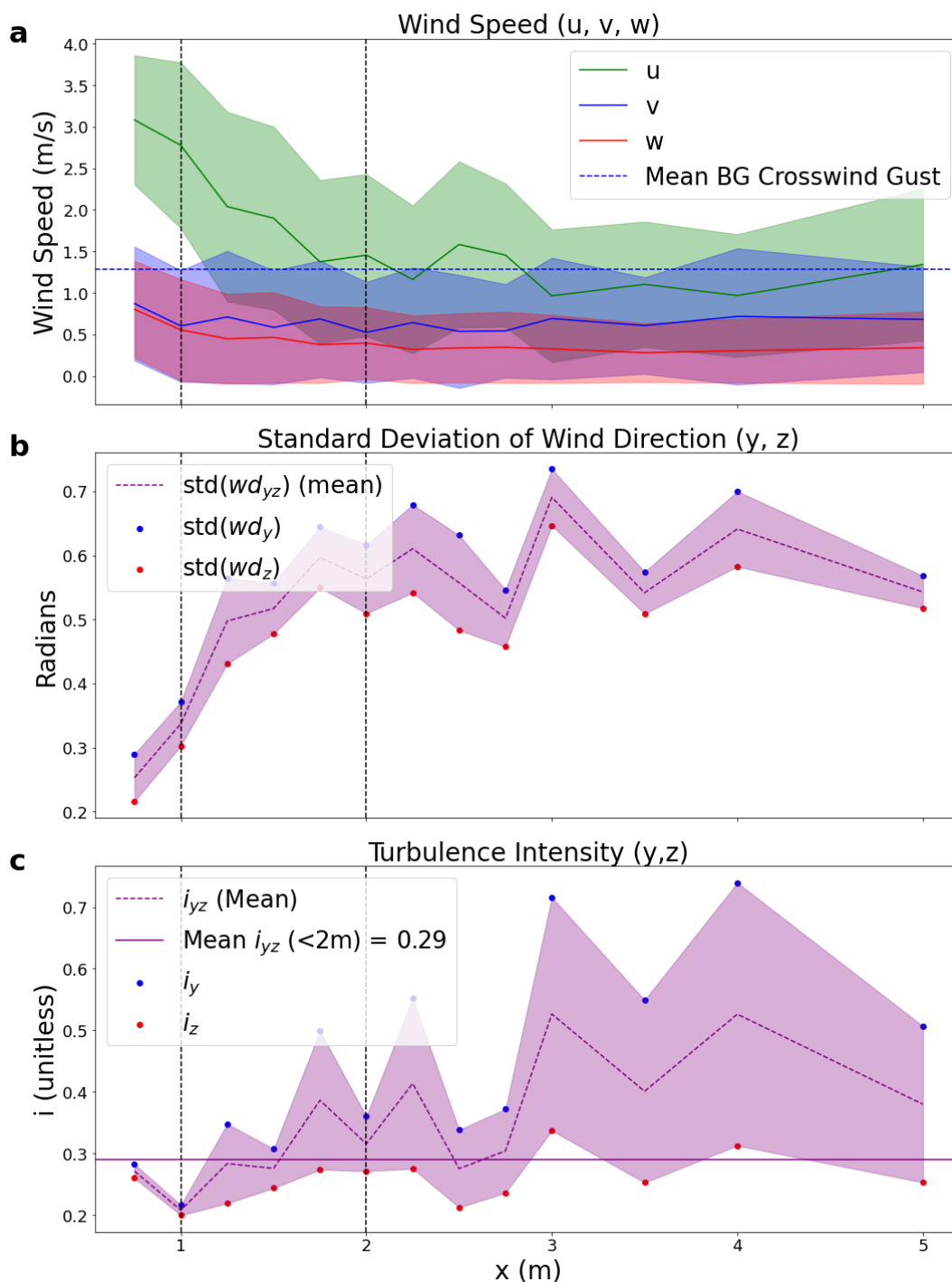
The measurement principle of the SEMTECH HI-FLOW relies on simultaneous measurements of air flow and methane concentration. If F_{air} is the volumetric flow rate of air captured by the system (in LPM), C is the concentration of methane in ppm, $C_{\text{background}}$ is the concentration of methane of the background, and $K(T,P,\eta)$ an adjustment parameter varying with temperature (T), pressure (P), air viscosity(η), then we can express the volumetric flow rate of methane F_{CH_4} as:

$$F_{\text{CH}_4} = F_{\text{air}} \cdot (C - C_{\text{background}}) \cdot K(T,P,\eta) \quad (\text{B1})$$

The velocity of the air is measured using a pitot tube, and the concentration of methane is measured using a gas analyzer (near-IR laser absorption CH_4 sensor sensitive on a range of 10 ppm to 100% of CH_4) located in the backpack. All other parameters such as temperature and pressure are also measured by the SEMTECH directly in the pitot tube. This system is designed to be user friendly, as the flow measured is directly shown on the system monitor. Data are logged every second (1Hz). For example as we can see in Figures B1 and B2, the SEMTECH measures the CH_4 emission rate, at a rate of one point per second, and returns a value in liters per minute (LPM) which we converted to g/h for more convenient use.

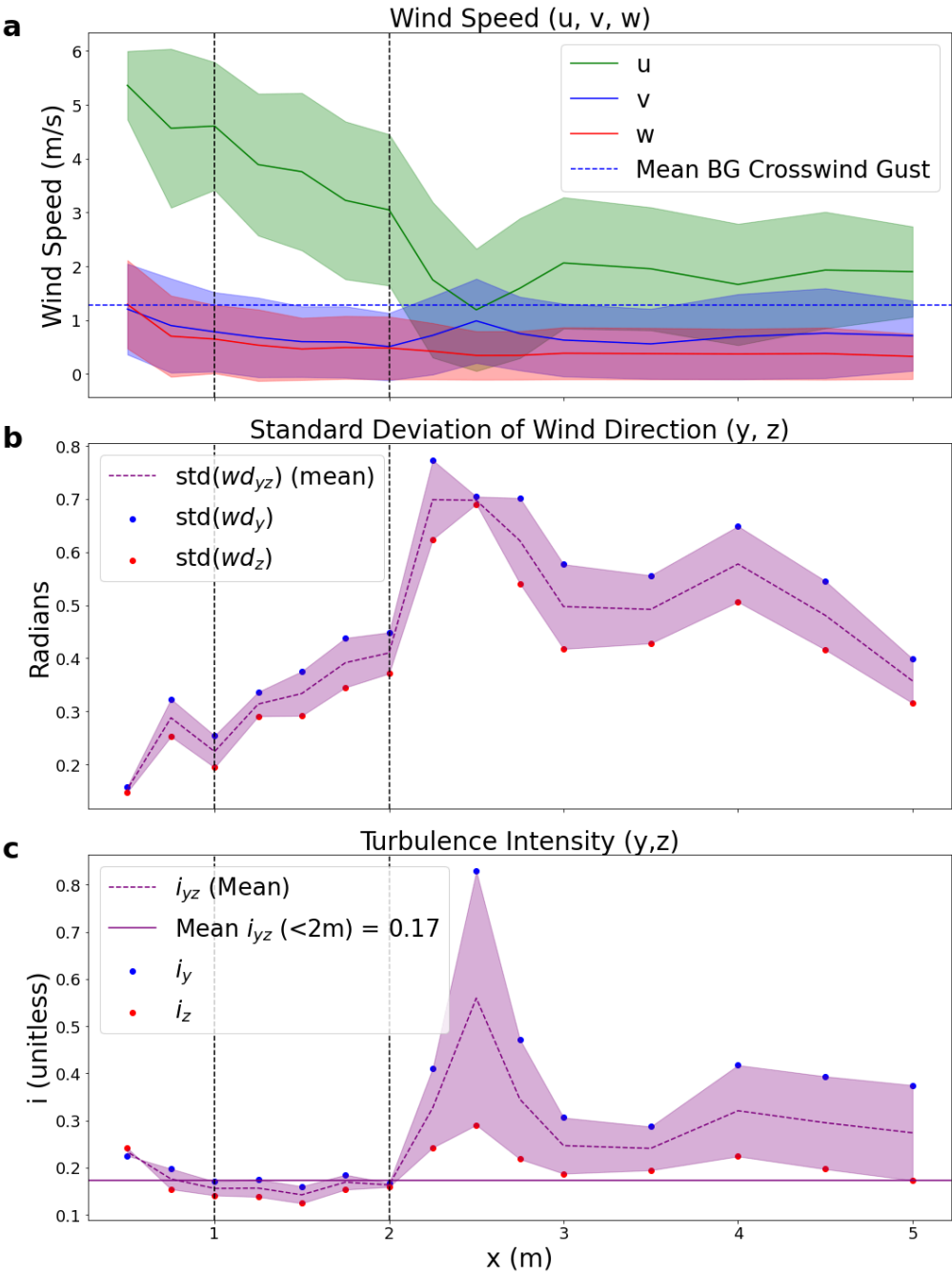






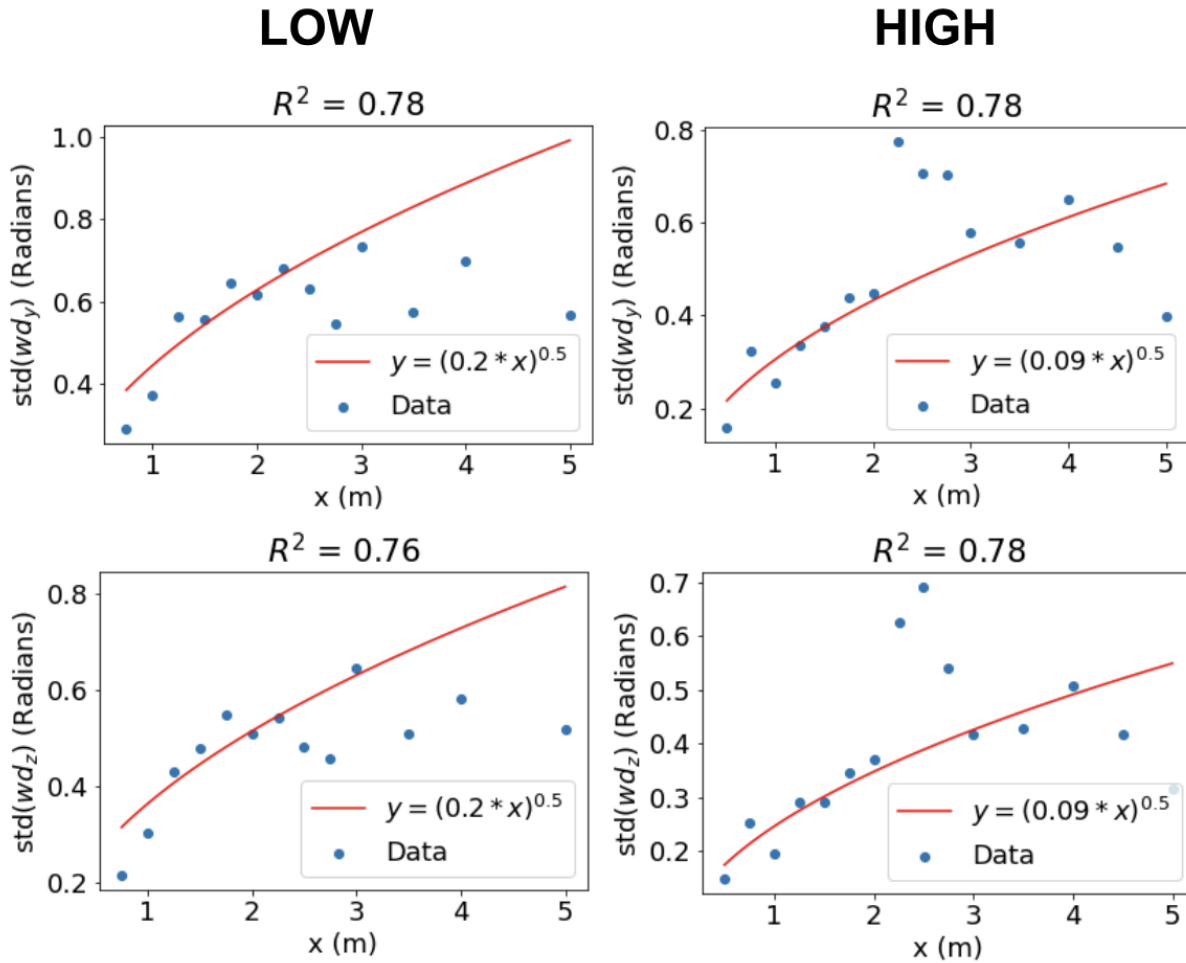
638
 639 **Figure C1:** a) Wind speed, b) standard deviation of wind direction, and c) turbulence intensity as a function of downwind
 640 distance x for Experiment 1 using the Low fan speed setting. Data are filtered to remove any points coming from the
 641 negative x direction (180 degrees)

642



643

644 **Figure C2:** a) Wind speed, b) standard deviation of wind direction, and c) turbulence intensity of Experiment 1 using the
645 High fan speed setting. Data are filtered to remove any points coming from the negative x direction (180 degrees)



646

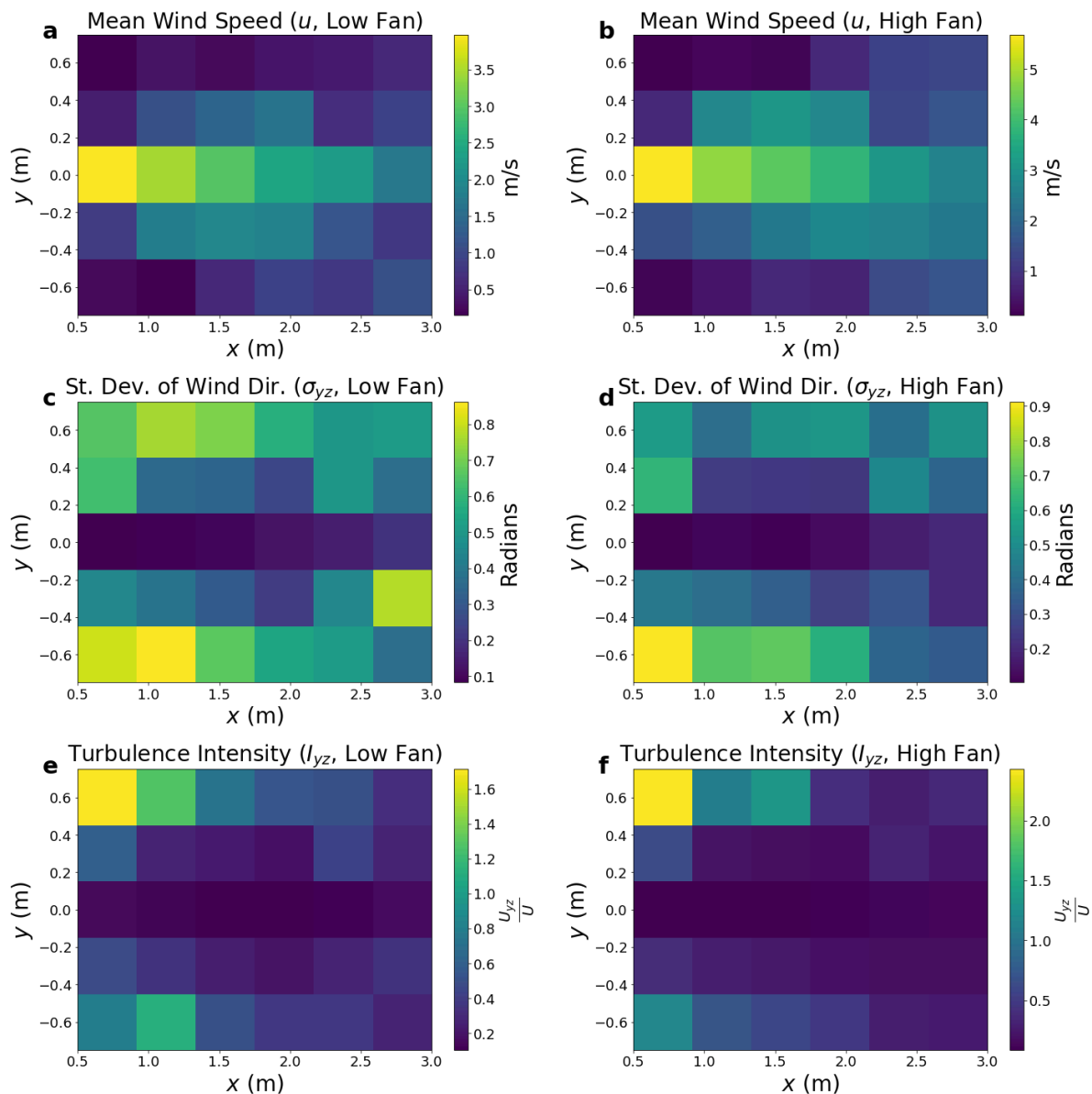
647 **Figure C3:** Square root fits to the standard deviations (std) of wind direction with filter angle = 180 degrees as expected by
 648 equation 2. The fits are valid in the range of 1-2 meters and depart from the square-root curve at larger downwind distances.

649

650

The results of the first fan characterization experiment are summarized in Figures C1-3. Figures C1 and C2 show
 651 the mean wind speed in 3D (u , v , w), standard deviation of wind direction in the x-y ($\text{std}(wd_y)$) and x-z ($\text{std}(wd_z)$) planes and
 652 turbulence intensity in the y (i_y) and z (i_z) directions at the range of downwind distances (x) for the Low and High fan speeds
 653 respectively. For both fan speeds, the u component of the flow starts higher than the background and decreases nearly
 654 linearly with distance until it is on the same order of magnitude as the background crosswind gust intensity (blue dashed
 655 line). The $\text{std}(wd_y)$ and $\text{std}(wd_z)$ values are calculated using the Yamartino method [Turner, 1986] and act as an estimate of
 656 the effective width of the plume (in radians). According to Equation 2, these should both therefore grow proportional to $x^{0.5}$,
 657 which is verified for $x < 2$ meters in Figure C3. The turbulence intensities (i_y) and (i_z) are calculated using the means of the
 658 magnitudes of u , v and w as $\text{mean}(v)/\text{mean}(u)$ and $\text{mean}(w)/\text{mean}(u)$ respectively. These should be relatively constant for the
 659 fan generated flow (i_{fan}) and about equal if the turbulence of the flow is uniform. The uniform flow near the fan is much more
 660 evident in the High fan data (Figure C2), whereas the Low fan measurements (Figure C1) indicate the effects of crosswind
 661 turbulence, resulting in much larger values of i_y compared to i_z . It is also important to note that during the measurement

662 period for the High fan speed, the crosswinds far exceeded their background value, resulting in a total disruption of the
 663 plume in this region ($2\text{ m} < x < 3\text{ m}$). The crosswinds died down later in the experiment when the anemometer was further
 664 downwind, resulting in a more stable plume for $x > 3\text{ m}$. Overall, we found that the fan plume remained stable to a wide
 665 range of crosswind conditions in the range of $1\text{ m} < x < 2\text{ m}$.
 666
 667



668
 669 **Figure C4:** a-b) Mean wind speed, c-d) standard deviation of wind direction in the x-y plane, and e-f) turbulence intensity in
 670 the y-z plane of Experiment 2 for low-fan setting (left) and high-fan setting (right).
 671

672 The results of the second fan characterization experiment are summarized in Figure C4. Similar to Figure C1, the
673 top row shows the mean wind speed in the downwind direction (u), the mean of standard deviation of wind direction in the
674 x-y ($\text{std}(wd_y)$) and x-z ($\text{std}(wd_z)$) planes, and the mean of the turbulence intensity in the y (i_y) and z (i_z) directions at a range
675 of downwind distances (x) and crosswind distances (y) for the Low and High fan speeds (left and right, respectively). Unlike
676 the first experiment, these measurements allowed for variation in both x and y , allowing us to investigate the shape of the
677 plume. The experiment was done with very little background wind (before sunrise) and in a location shielded from crosswind
678 on one side by a wall (Fig. 2). The measurements were taken at 10 Hz for 1 minute intervals at each of the points in the x-y
679 grid (0.5 m intervals in x for $0.5 < x < 3.0$ and 0.33 m intervals in y for $-0.66 < y < 0.66$) as depicted in Figure C4.

680

681 From these measurements, the MDB fan was able to generate a jet of pseudo-homogeneous turbulence at a range of
682 downwind distances between 1 and 2 meters. Beyond 2 meters, the plume becomes unstable and can be broken easily by
683 crosswinds, even at a High fan setting. Furthermore, the heat maps in Figure C4 also point to the importance of measuring
684 along the centerline ($y = 0$), as the effects of crosswind turbulence increase by a large amount even when only slightly off of
685 the centerline ($y > 0.3$ m). Based on these results, the controlled release experiment was conducted with the sensors at a
686 distance of 2 meters from the fan, and all of the field measurements were performed with a distance of less than 2 meters.

687

688

689 **Code/Data Availability**

690 All relevant code and data is available upon request from the corresponding author.

691

692 **Author contribution:**

693 Mohit L. Dubey: Conceptualization, Data curation, Formal analysis, Investigation, Methodology, Software, Validation,
694 Visualization, Writing

695 Andre Santos: Conceptualization, Data curation, Investigation, Methodology, Validation, Visualization, Writing

696 Andrew B. Moyes: Conceptualization, Investigation, Methodology, Validation, Writing (review and editing)

697 Ken Reichl: Conceptualization, Data curation, Investigation, Methodology, Validation, Writing

698 James E. Lee: Investigation, Writing (review and editing)

699 Manvendra K. Dubey: Investigation, Writing (review and editing)

700 Corentin LeYhuelic: Investigation, Formal analysis, Writing (review and editing)

701 Evan Variano: Formal analysis

702 Emily Follansbee: Investigation, Writing (review and editing)

703 Fotini K. Chow: Conceptualization, Formal analysis, Writing (review and editing)

704 Sébastien C. Biraud: Conceptualization, Investigation, Methodology, Validation, Writing (review and editing), Project
705 administration, Funding acquisition

706

707 **Competing interests:**

708 The authors declare that they have no conflict of interest.

709 Acknowledgements

710 This work was supported as part of the Consortium Advancing Technology for Assessment of Lost Oil & Gas, funded by the
711 U.S. Department of Energy, Office of Fossil Energy and Carbon Management, Office of Resource Sustainability, Methane
712 Mitigation Technologies Division's, Undocumented Orphan Wells Program. This material is based upon work supported by
713 the U.S. Department of Energy, Office of Science, Office of Advanced Scientific Computing Research, Department of
714 Energy Computational Science Graduate Fellowship under Award Number(s) Grant Number: DE-SC0024386)]. Authors at
715 Lawrence Berkeley National Laboratory are supported under Contract No. DE-AC02-05CH11231 with the U.S. Department
716 of Energy. The U.S. Government retains, and the publisher, by accepting the article for publication, acknowledges that the
717 U.S. Government retains a non-exclusive, paid-up, irrevocable, world-wide license to publish or reproduce the published
718 form of this manuscript, or allow others to do so, for U.S. Government purposes. We also thank the people of the Osage
719 Nation, Oklahoma, for providing access to their field sites and the US Forest Service for hosting the Lufkin, TX sampling.

720 References

- 721 Cooper, C. D. and Alley, F. C.: Air Pollution Control: A Design Approach, 4th ed., Waveland Press, Inc., Long Grove, IL,
722 pp. 662-663 pp., 2011.
- 723 Biden-Harris Administration Invests \$660 Million for States to Plug Orphaned Oil and Gas Wells through President's
724 Investing in America Agenda | U.S. Department of the Interior:
725 <https://www.doi.gov/pressreleases/biden-harris-administration-invests-660-million-states-plug-orphaned-oil-and-gas-wells>,
726 last access: 15 May 2024.
- 727 Dooley, J. F., Minschwaner, K., Dubey, M. K., El Abbadi, S. H., Sherwin, E. D., Meyer, A. G., Follansbee, E., and Lee, J. E.:
728 A New Technique for Airborne Measurements to Quantify Methane Emissions Over a Wide Range: Implementation and
729 Validation, <https://doi.org/10.5194/egusphere-2024-760>, 19 March 2024.
- 730 Dubey, M., Meyer, A., Dubey, M., Pekney, N., O'Malley, D., Viswanathan, H., Govert, A., and Biraud, S.: How to estimate
731 O&G well leak rates from near field concentration and wind observations?, <https://doi.org/10.2172/1922013>, 2023.
- 732 Edie, R., Robertson, A. M., Field, R. A., Soltis, J., Snare, D. A., Zimmerle, D., Bell, C. S., Vaughn, T. L., and Murphy, S. M.:
733 Constraining the accuracy of flux estimates using OTM 33A, Atmospheric Measurement Techniques, 13, 341–353,
734 <https://doi.org/10.5194/amt-13-341-2020>, 2020.
- 735 Follansbee, E., Lee, J. E., Dubey, M. L., Dooley, J., Schuck, C., Minschwaner, K., Santos, A., Biraud, S. C., and Dubey, M.
736 K.: Quantifying Methane Fluxes from Super-Emitting Orphan Wells to Report Carbon Credits and Prioritize Remediation,
737 <https://doi.org/10.22541/essoar.171781163.39594276/v1>, 8 June 2024.

738 Halloran, S. K., Wexler, A. S., and Ristenpart, W. D.: Turbulent dispersion via fan-generated flows, *Phys Fluids* (1994), 26,
739 055114, <https://doi.org/10.1063/1.4879256>, 2014.

740 Methane Tracker 2020 – Analysis: <https://www.iea.org/reports/methane-tracker-2020>, last access: 24 January 2025.

741 IOGCC: IDLE AND ORPHAN OIL AND GAS WELLS: STATE AND PROVINCIAL REGULATORY STRATEGIES,
742 2021.

743 Kang, M., Boutot, J., McVay, R. C., Roberts, K. A., Jasechko, S., Perrone, D., Wen, T., Lackey, G., Raimi, D., Digiulio, D.
744 C., Shonkoff, S. B. C., William Carey, J., Elliott, E. G., Vorhees, D. J., and Peltz, A. S.: Environmental risks and
745 opportunities of orphaned oil and gas wells in the United States, *Environ. Res. Lett.*, 18, 074012,
746 <https://doi.org/10.1088/1748-9326/acdae7>, 2023.

747 Lushi, E. and Stockie, J. M.: An inverse Gaussian plume approach for estimating atmospheric pollutant emissions from
748 multiple point sources, *Atmospheric Environment*, 44, 1097–1107, <https://doi.org/10.1016/j.atmosenv.2009.11.039>, 2010.

749 Merrill, M. D., Grove, C. A., Gianoutsos, N. J., and Freeman, P. A.: Analysis of the United States documented unplugged
750 orphaned oil and gas well dataset, U.S. Geological Survey, <https://doi.org/10.3133/dr1167>, 2023.

751 O’Malley, D., Delorey, A. A., Guiltinan, E. J., Ma, Z., Kadeethum, T., Lackey, G., Lee, J., E. Santos, J., Follansbee, E., Nair,
752 M. C., Pekney, N. J., Jahan, I., Mehana, M., Hora, P., Carey, J. W., Govert, A., Varadharajan, C., Ciulla, F., Biraud, S. C.,
753 Jordan, P., Dubey, M., Santos, A., Wu, Y., Kneafsey, T. J., Dubey, M. K., Weiss, C. J., Downs, C., Boutot, J., Kang, M., and
754 Viswanathan, H.: Unlocking Solutions: Innovative Approaches to Identifying and Mitigating the Environmental Impacts of
755 Undocumented Orphan Wells in the United States, *Environ. Sci. Technol.*, 58, 19584–19594,
756 <https://doi.org/10.1021/acs.est.4c02069>, 2024.

757 Perry, S. G., Cimorelli, A. J., Paine, R. J., Brode, R. W., Weil, J. C., Venkatram, A., Wilson, R. B., Lee, R. F., and Peters, W.
758 D.: AERMOD: A Dispersion Model for Industrial Source Applications. Part II: Model Performance against 17 Field Study
759 Databases, *Journal of Applied Meteorology*, 44, 694–708, <https://doi.org/10.1175/JAM2228.1>, 2005.

760 GasScouterTM G4302 Mobile Gas Concentration Analyzer | Picarro:
761 https://www.picarro.com/environmental/products/gasscoutertm_g4302_mobile_gas_concentration_analyzer, last access: 7
762 January 2025.

763 Porter, J. G., De Bruyn, W., and Saltzman, E. S.: Eddy flux measurements of sulfur dioxide deposition to the sea surface,
764 *Atmos. Chem. Phys. Discuss.* [preprint], <https://doi.org/https://doi.org/10.5194/acp-18-15291-2018>, 13 June 2018.

765 Riddick, S. N., Mauzerall, D. L., Celia, M. A., Kang, M., and Bandilla, K.: Variability observed over time in methane
766 emissions from abandoned oil and gas wells, *International Journal of Greenhouse Gas Control*, 100, 103116,
767 <https://doi.org/10.1016/j.ijggc.2020.103116>, 2020.

768 Riddick, S. N., Ancona, R., Mbua, M., Bell, C. S., Duggan, A., Vaughn, T. L., Bennett, K., and Zimmerle, D. J.: A
769 quantitative comparison of methods used to measure smaller methane emissions typically observed from superannuated oil
770 and gas infrastructure, *Atmos. Meas. Tech.*, 15, 6285–6296, <https://doi.org/10.5194/amt-15-6285-2022>, 2022.

771 Riddick, S. N., Mbua, M., Riddick, J. C., Houlihan, C., Hodshire, A. L., and Zimmerle, D. J.: Uncertainty Quantification of
772 Methods Used to Measure Methane Emissions of 1 g CH₄ h⁻¹, *Sensors*, 23, 9246, <https://doi.org/10.3390/s23229246>, 2023.

773 Riddick, S. N., Mbua, M., Santos, A., Emerson, E. W., Cheptonui, F., Houlihan, C., Hodshire, A. L., Anand, A., Hartzell, W.,
774 and Zimmerle, D. J.: Methane emissions from abandoned oil and gas wells in Colorado, *Science of The Total Environment*,
775 922, 170990, <https://doi.org/10.1016/j.scitotenv.2024.170990>, 2024.

776 Saint-Vincent, P. M. B., Reeder, M. D., Sams, J. I., and Pekney, N. J.: An Analysis of Abandoned Oil Well Characteristics
777 Affecting Methane Emissions Estimates in the Cherokee Platform in Eastern Oklahoma, *Geophysical Research Letters*, 47,
778 e2020GL089663, <https://doi.org/10.1029/2020GL089663>, 2020.

779 Sánchez-Sosa, J. E., Castillo-Mixcóatl, J., Beltrán-Pérez, G., and Muñoz-Aguirre, S.: An Application of the Gaussian Plume
780 Model to Localization of an Indoor Gas Source with a Mobile Robot, *Sensors (Basel)*, 18, 4375,
781 <https://doi.org/10.3390/s18124375>, 2018.

782 SEMTECH HI-FLOW 2: https://sensors-inc.com/Products/Custom_Solutions/SEMTECH_HI-FLOW_2, last access: 27 June
783 2024.

784 Sherwin, E. D., Rutherford, J. S., Zhang, Z., Chen, Y., Wetherley, E. B., Yakovlev, P. V., Berman, E. S. F., Jones, B. B.,
785 Cusworth, D. H., Thorpe, A. K., Ayasse, A. K., Duren, R. M., and Brandt, A. R.: US oil and gas system emissions from
786 nearly one million aerial site measurements, *Nature*, 627, 328–334, <https://doi.org/10.1038/s41586-024-07117-5>, 2024.

787 Snoun, H., Krichen, M., and Chérif, H.: A comprehensive review of Gaussian atmospheric dispersion models: current usage
788 and future perspectives, *Euro-Mediterr J Environ Integr*, 8, 219–242, <https://doi.org/10.1007/s41207-023-00354-6>, 2023.

789 Taylor, G. I.: Diffusion by Continuous Movements, *Proceedings of the London Mathematical Society*, s2-20, 196–212,
790 <https://doi.org/10.1112/plms/s2-20.1.196>, 1922.

791 UN Climate Change Global Innovation Hub COP26 Event Report: <https://unfccc.int/documents/460986>, last access: 25
792 September 2024.

793 U.S. EPA: Other Test Method – 34: Method to Quantify Road Dust Particulate Matter Emissions (PM₁₀ and/or PM_{2.5}) from
794 Vehicular Travel on Paved and Unpaved Roads, 2014.

795 Veigele, Wm. J. and Head, J. H.: Derivation of the Gaussian Plume Model, *Journal of the Air Pollution Control Association*,
796 28, 1139–1140, <https://doi.org/10.1080/00022470.1978.10470720>, 1978.

797 Achieve Net-Zero with Ventsentinel®: Revolutionizing Methane Emission Monitoring:
 798 <https://www.ventbusters.com/updates/2023/11/10/greenhouse-gas-emission-monitoring-with-the-ventsentinel-a-revolutionar>
 799 [y-advancement-in-continuous-vent-gas-quantification](#), last access: 25 September 2024.

800 Williams, J. P., Regehr, A., and Kang, M.: Methane Emissions from Abandoned Oil and Gas Wells in Canada and the United
 801 States, *Environ. Sci. Technol.*, 55, 563–570, <https://doi.org/10.1021/acs.est.0c04265>, 2021.

802 Williams, J. P., El Hachem, K., and Kang, M.: Controlled-release testing of the static chamber methodology for direct
 803 measurements of methane emissions, *Atmos. Meas. Tech.*, 16, 3421–3435, <https://doi.org/10.5194/amt-16-3421-2023>, 2023.

804 Zeng, Y. and Morris, J.: Detection limits of optical gas imagers as a function of temperature differential and distance, *Journal*
 805 *of the Air & Waste Management Association*, 69, 351–361, <https://doi.org/10.1080/10962247.2018.1540366>, 2019.